Design, Synthesis, Biological Evaluation of Novel Small Molecule Inhibitors for Early Diagnosis and Therapy of Prostate Cancer

M.Sc. Thesis

By

Saroj Ali

DEPARTMENT OF CHEMISTRY

INDIAN INSTITUTE OF TECHNOLOGY INDORE

May 2022

Design, Synthesis, Biological Evaluation of Novel Small Molecule Inhibitors for Early Diagnosis and Therapy of Prostate Cancer

A THESIS

Submitted in partial fulfillment of the requirements for the award of the degree of

Master of Science

By

Saroj Ali

DEPARTMENT OF CHEMISTRY

INDIAN INSTITUTE OF TECHNOLOGY INDORE

May 2022

INDIAN INSTITUTE OF TECHNOLOGY INDORE

CANDIDATE'S DECLARATION

I hereby certify that the work which is being presented in the thesis entitled **Design, Synthesis, Biological Evaluation of Novel Small Molecule Inhibitors for Early Diagnosis and Therapy of Prostate Cancer** in the partial fulfillment of the requirements for the award of the degree of **MASTER OF SCIENCE** and submitted in the **DEPARTMENT OF CHEMISTRY, Indian Institute of Technology Indore**, is an authentic record of my own work carried out during the period from July 2021 to May 2022 under the supervision of Dr. Venkatesh Chelvam, Associate Professor, IIT Indore.

The matter presented in this thesis has not been submitted by me for the award of any other degree of this or any other institute.

Saroj Ali

25.05.2022

Saroj Ali

This is to certify that the above statement made by the candidate is correct to the best of my knowledge.

Venkatesh C

25.05.2022

Dr. Venkatesh Chelvam

Saroj Ali has successfully given her M.Sc. Oral Examination held on **May 25, 2022**

Venkatesh C

Signature of Supervisor of M.Sc. thesis
Dr. Venkatesh Chelvam
Date: 25.05.2022

Tushar Kanti Mukherjee

Convener, DPGC
Dr. Tushar Kanti Mukherjee
Date: 25.05.2022

Sampanta

Signature of PSPC Member
Prof. Sampak Samanta
Date: 25.05.2022

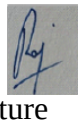

Signature of PSPC Member
Prof. Rajneesh Misra
Date: 25.05.2022

ACKNOWLEDGEMENT

It would be my great pleasure to offer appreciation to Dr. Venkatesh Chelvam for his great guidance and valuable suggestion throughout this whole course. His efforts were the fuel to my work that happened so smoothly.

I am sincerely thankful to the Department of Chemistry and IIT Indore for providing me with the opportunity to pursue my M.Sc. Project.

I would like to express my respect to PSPC members Prof. Rajneesh Misra and Prof. Sampak Samanta. I would also like to acknowledge Prof. Biswarup Pathak (Head, Department of Chemistry) and Dr. Tushar Kanti Mukherjee (DPGC Convener) for their suggestion and guidance.

I am also thankful to my lab members Dr. Mena Asha Krishnan, Ms. Kratika Yadav, Mr. Lekhnath Sharma, Mr. Soumit Dutta, Mr. Tapash Kalita and Ms. Antim Rani. With their support and constant effort, I was able to conduct my work quite easily and confidently.

I am thankful to the technical staff of Sophisticated Instrumentation Centre (SIC), IIT Indore Mr. Kinny Pandey, Mr. Ghanshyam Bhavsar and Chemistry Office staff Mr. Manish Kushwaha, Mr. Parthiban, Mr. Rameshwar Dohare and Ms. Vinita Kothari for their help and support.

Finally, I would like to acknowledge IIT Indore for providing infrastructure and all the facilities needed to carry out my research work efficiently and smoothly.

ABSTRACT

19.3 million new cancer cases and 10 million cancer deaths are reported worldwide in the year 2020. In the male population, prostate cancer (PCa), is the second most diagnosed cancer. PSMA is a membrane-bound protein and is an important target to identify prostate cancer at an early stage. It is overexpressed 100 to 1000-fold in cancerous tissues than that of the normal or healthy cells. In this study, we have designed ten aminoacetamide-based ligands to target PSMA protein. Molecular docking studies were performed to identify potent ligands, and currently, we are synthesizing the new ligands. The best among the designed ligands will be used in solid phase peptide methodology to synthesize bioconjugates that can be attached to a fluorescent reporter, rhodamine B or chelating moiety to deliver radioisotopes such as ^{99m}Tc for early diagnosis of PCa. The bioconjugates have potential applications for performing diagnosis and intraoperative fluorescence-guided surgery (FGS) of PCa.

TABLE OF CONTENTS

LIST OF FIGURES

LIST OF SCHEMES

LIST OF TABLES

ACRONYMS

Abbreviations used for amino acids, substituents, reagents etc. are largely in accordance with the recommendation of the IUPAC-IUB Commission on Biochemical Nomenclature, 1974, Pure and Applied Chemistry, 40, 315-331. All amino acids have L-configuration. Standard three-letter code is used for all amino acids. Additional abbreviations used in this report are listed below:

Asp	Aspartic acid
Arg	Arginine
DCC	Dicyclohexyl carbodiimide
DNA	Deoxyribonucleic acid
FGS	Fluorescence guided surgery
Glu	Glutamic acid
His	Histidine
HOBt	Hydroxybenzotriazole
Lys	Lysine
MRSI	Magnetic resonance spectroscopic imaging
NAAG	N-Acetylaspartyl glutamate
PSMA	Prostate specific membrane antigen
PET	Positron emission tomography
Ser	Serine
SPECT	Single photon emission computed tomography
TFA	Trifluoroacetic acid
TIPS	Triisopropylsilane

Tyr	Tyrosine

Chapter 1

INTRODUCTION

1.1 Cancer and its statistics

Cancer cells are different from normal cells in terms of their cell division which is extremely fast and hence proliferates unrestrictedly. When this tendency of cell division spreads in the body to other distant organs, it is called cancer metastasis. There may be different causes of initiation of cancer some of which are caused by external factors like tobacco chewing, exposure to radiation and chemicals, and internal factors such as inherited mutation. Database from GLOBOCAN 2020 report shows that 19.3 million new cancer cases and 10 million cancer deaths are reported worldwide [1]. In the male population, prostate cancer (PCa) is the second most diagnosed cancer after lung cancer [1].

Table 1. GLOBOCAN 2020, incidence and mortality [1]

Cancer site	No. of cases (% of all sites)	No. of deaths (% of all sites)
Female breast	2,261,419 (11.7)	684,996 (6.9)
Lung	2,206,771 (11.4)	1,796,144 (18.0)
Prostate	1,414,259 (7.3)	375,304 (3.8)

1.2 Conventional therapy of cancer

There are several conventional approaches to treat cancer. Surgery, chemotherapy, and radiotherapy are most often practiced by physicians in India for the treatment of cancer.

Surgery: The best result is found in surgery when cancer has not spread to distant organs. But unfortunately, when cancers are diagnosed, they are in advanced stage and difficult to treat by surgery alone. Moreover, there is always a chance for recurrence of the disease even after surgery.

Chemotherapy: The cytotoxic drugs can be used for metastasis because the effect of these drugs is not localized. The drugs can destroy cancer cells in distant organs.

Chemotherapy can be either neoadjuvant (shrinking down of the tumor lesions before surgery or radiotherapy) or adjuvant chemotherapy (remaining cancer cells are killed after surgery or radiotherapy). But, because of its almost indiscriminating property between healthy and cancer cells, the cytotoxic drugs act upon the healthy cells also and cause various side effects.

Radiotherapy: Radiation therapy prevents cancer cell divisions and does not allow cancer cells to grow and proliferate. Almost 50% of the patients suffering from cancer receive radiotherapy [2].

1.3 Biomarkers and targeted delivery

Most of the abnormal cells overexpress membrane proteins that have a high affinity for their naturally occurring inhibitors or ligands to grow and proliferate faster. These proteins are called biomarkers. When radionuclides or fluorescent probes are attached to these ligands and bind to the biomarkers, healthy cells can be differentiated from diseased cells. Receptor-mediated delivery of cargos can minimize the damage to healthy cells [3]. Using this phenomenon, many diagnostic methods like PET, SPECT, MRSI, optical imaging, and radio nuclear imaging have been developed.

1.4 Molecular imaging probe

Molecular imaging probes are useful to observe tissue and biomarkers overexpressed on the cell membrane. A molecular imaging probe contains targeting moiety (which can bind to the biomarker), a linker (which connects the signaling agent to targeting moiety), and a signaling agent from which images are obtained [4]. There are some characteristic features that make molecular imaging probes highly useful for imaging purposes. First, the tendency of the imaging probe to bind to the target should be high i.e., rate of association of probe with binding target must be much higher than the rate of dissociation. A high affinity constant will make a probe sensitive wherein a minimal amount of probe will be required to produce an image. Second, the probe should be highly selective so that it doesn’t bind to the healthy cells and provide a high contrast image of the diagnosed organ. Third, it should have higher stability in vivo, low toxicity, and be affordable for wide use.

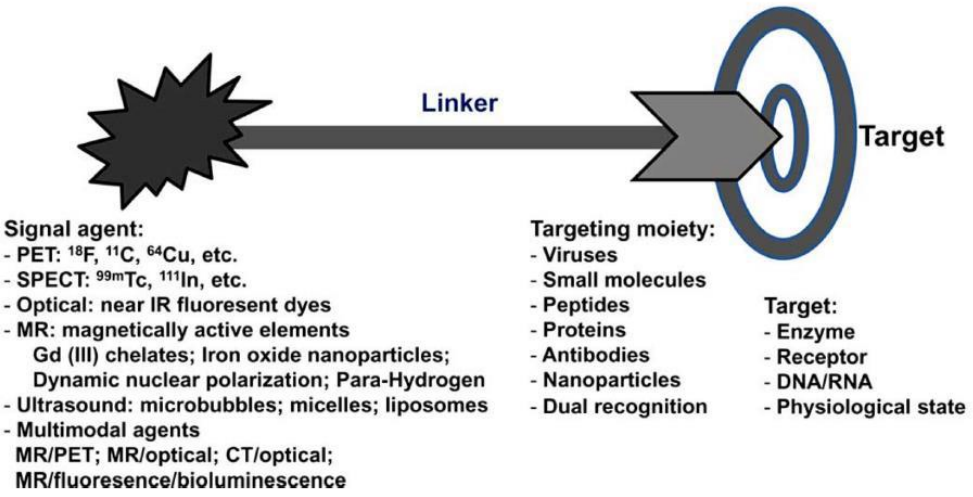

Figure 1. Schematic representation of molecular imaging probes

1.5 Prostate cancer

In the United States from the year of 2015 to 2017, it was found that in the age range of 70 to older, one person among twelve people has prostate cancer and in the age range of 60 to 69, one person among twenty people was reported having prostate cancer [5]. In India, at the age range of 70 years, one person among 125 people was reported as having prostate cancer in the year 2020 [6]. Prostate cancer spreads to the distant organ, and to the bone and causes pain and disability [7]. In the advanced stage of PCa people suffer from muscle waste, cognitive decline, osteoporosis, and in case of biological recurrence people suffer from sexual dysfunction and incontinence, feel pain, anger, and decreased mental health, thereby quality of life decreases [8]. There are several diagnostic tests for prostate cancer like digital rectal examination (DRE), prostate-specific antigen (PSA) test, and biopsy guided by ultrasound [9]. But none of these tests are not very effective because of their disadvantages.

1.6 PSMA

For imaging and therapy of PCa, prostate specific membrane antigen (PSMA) is a popular target as it is a cell membrane protein and overexpressed about 100 to 1000-fold in cancerous cells than that of normal tissues such as small intestine, kidney, and salivary gland [10]. PSMA is also found in epithelial cells of the prostate gland [11]. It is a binuclear zinc peptidase and known as N-acetyl-aspartyl-glutamate peptidase I

(NAAG peptidase I) or glutamate carboxypeptidase II (GCPII) or folate hydrolase 1 (FOLH 1). There are three distinct domains of glutamate carboxypeptidase II at the extracellular portion. They are protease domain (domain I) containing residues 57 to 116 and 352 to 590, the apical domain (domain II) containing residues 117 to 351, and the C-terminal domain containing residues 591 to 750 (Figure 2). The amino acids of these three domains recognize substrates. Figure 2 of GCPII shows a subunit in grey colour. Dark, green-colored spheres represent two Zn^{2+} ions, red-colored spheres represent Ca^{2+} ion and yellow-colored sphere represents chloride ion [12].

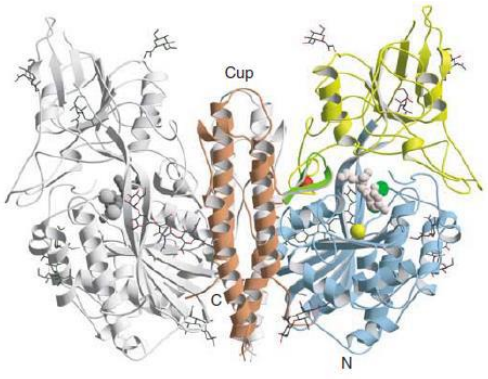

Figure 2. Structure of glutamate carboxypeptidase II (GCP II)

Figure 3 schematic representation shows that PSMA consists of a short NH_2- terminal cytoplasmic domain (CD), a hydrophobic transmembrane region (TM), and a large extracellular domain (ED). Alphabet Y indicates a highly glycosylated extracellular domain of PSMA [13]. PSMA transports substrate across the plasma membrane through clathrin-mediated endocytosis by recycling the receptors from the cytoplasm to the surface of the plasma membrane for the next rounds of uptake [14].

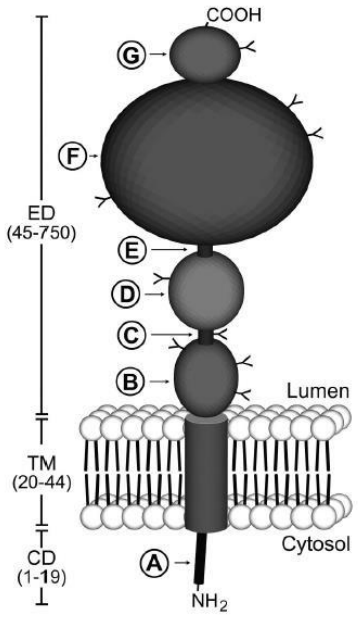

Figure 3. Schematic representation of PSMA

Folic acid is important for red blood corpuscles and for the repair and synthesis of RNA and DNA. On the other hand, N-acetylaspartyl glutamate (NAAG), which is found in the central nervous system, is an important neurotransmitter, the hydrolysis of which by PSMA will produce glutamate neurotransmitter. Excess glutamate, being an excitatory neurotransmitter, can cause damage to neurons resulting in neurological disorders. PSMA, which is also called folate hydrolase I, dissociates folyl-poly-γ-glutamate in the small intestine to generate glutamic acid and folate [15].

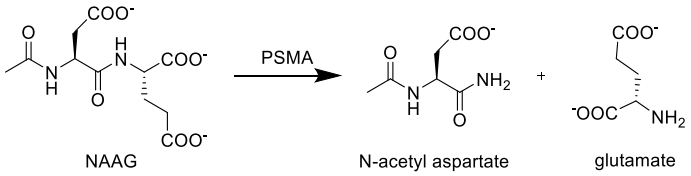

Figure 4. Hydrolysis of NAAG by PSMA

There are two subunits of PSMA when it acts as GCPII. One subunit is S1' which can recognize glutamate and the other one is S1 pocket which is amphiphilic in nature [16]. Near the S1 pocket, there is a 20 Å cylindrical deep tunnel that reaches the enzyme surface [11]. At the interface of two pockets S1 and S1' there are the two Zn^{2+} ions having coordination with five amino acid residues [11].

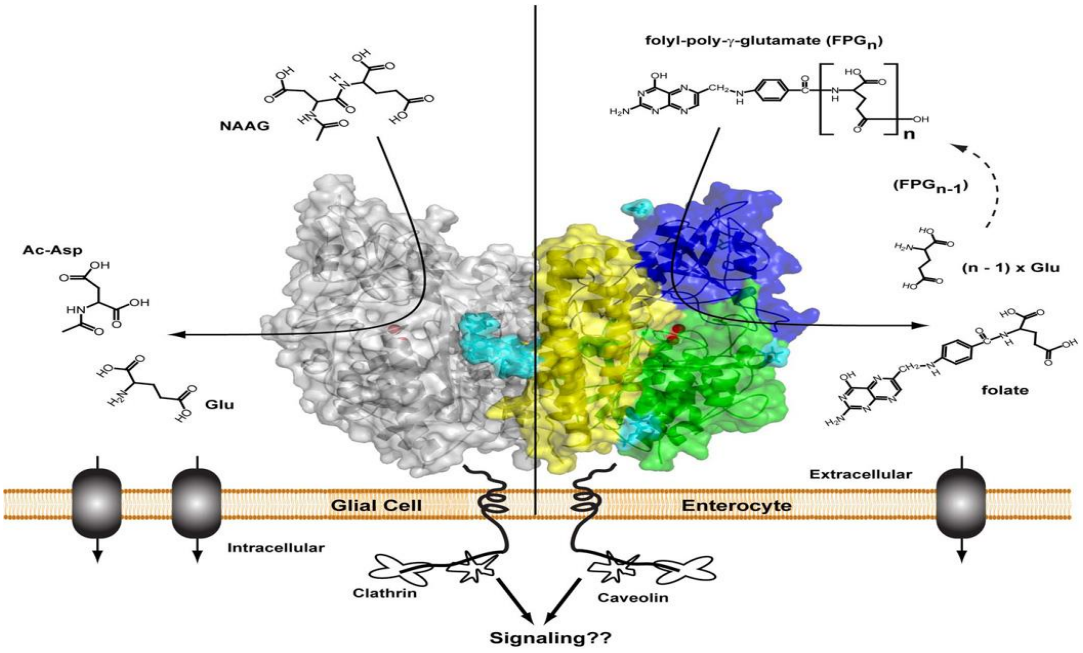

Figure 5. Biological function of prostate specific membrane antigen

Two Zn^{2+} ions which are active sites of PSMA are located at 20 Å tunnel deep inside the protein. In figure 6, aspartyl residue does not bind with the amino acid residues in the S1 pocket, whereas glutamate residue makes interaction with Lys699 and Tyr700 in the S1' pocket. Therefore, Lys699 and Tyr700 residues are also known as 'glutamate sensor' residues. Glu424 plays an important role in the hydrolysis of NAAG substrate. The water molecule is bridged between two Zn^{2+} ions and a hydrogen atom of the water molecule is involved in hydrogen bonding with the carbonyl oxygen of Glu424 carboxylate residue and the hydroxyl oxygen of Glu424 makes another H-bonding interaction with the glutamate -NH of NAAG. Next, Glu424 abstracts a proton from a water molecule to release hydroxyl anion for nucleophilic attack on the amide bond of NAAG substrate to produce N-acetyl aspartate and glutamate.

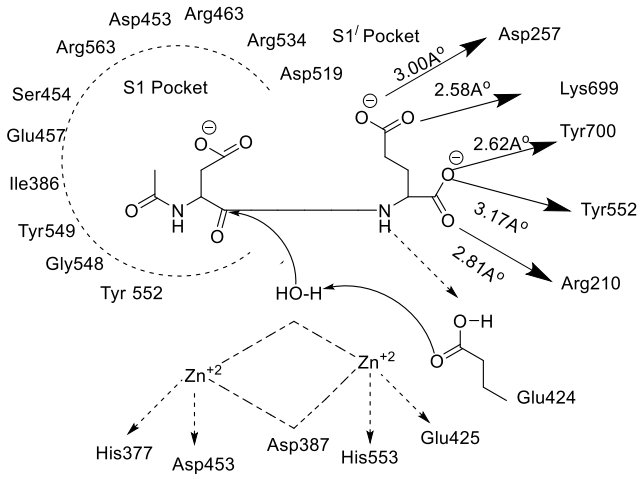

Figure 6. Activity of NAAG peptidase I

1.7 Project objectives

The objective of the project is to design, synthesize and perform a biological evaluation of novel small molecule inhibitors which will be used for early diagnosis and therapy of prostate cancer. We have designed aminoacetamide ligands based on molecular docking studies of inhibitors with PSMA protein that can be used for the synthesis of ligand-targeted bioconjugates for early diagnosis and therapy of PCa.

1.8 Retrosynthetic approach for the synthesis of designed aminoacetamide ligands

We have designed several aminoacetamide ligands and a retrosynthetic approach is shown in scheme 1. The aminoacetamide ligands **2a-j** can be derived from tris(*t*-butylcarboxy)benzyl carboxy-protected precursors **1a-j**. **1a-j** can be prepared from dicarboxy-protected glutamic acid **5** and α-bromoacetamide amino acids **3a-j** which in turn can be obtained from α-bromoacetic acid *t*-butylcarboxy amino acids **4a-j**.

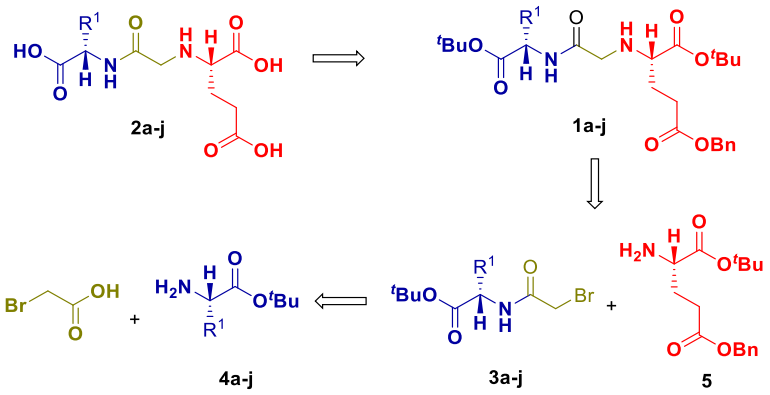

Scheme 1. Retrosynthesis for glutamic acid-based aminoacetamide ligands

1.9 Work plan

Initially, we plan to synthesize carboxylic acid-protected aminoacetamide-based small molecule inhibitors **1a-j** (Figure 7) using a methodology developed in our research group. Later the precursors **1a-j** can be deprotected to afford appropriate PSMA ligands **2a-j** (Figure 8). JB7 is considered a standard inhibitor of PSMA protein and molecular docking of **2a-j** is performed using JB7 as a reference ligand to determine docking scores. Based on docking scores, the best ligands or inhibitors will be selected for conjugation to prepare bioconjugates with a fluorescent reporter or chelating moiety to deliver radionuclides that can be used for diagnosis as well as therapy of PCa.

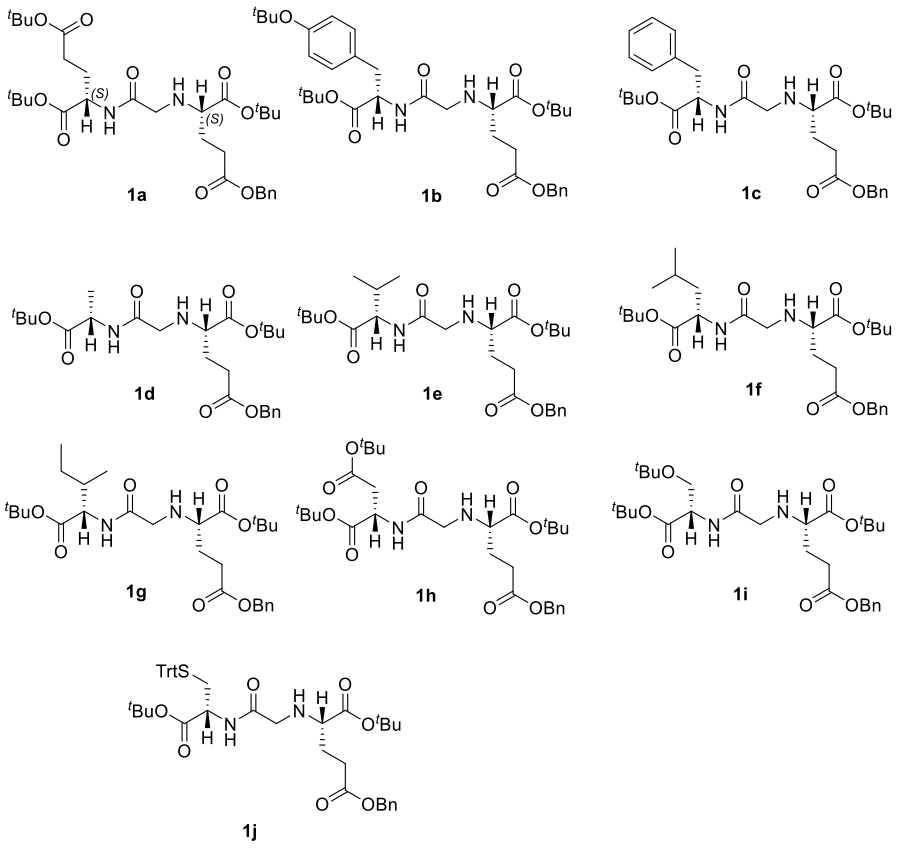

Figure 7. Designed aminoacetamide ligand precursors **1a-j**

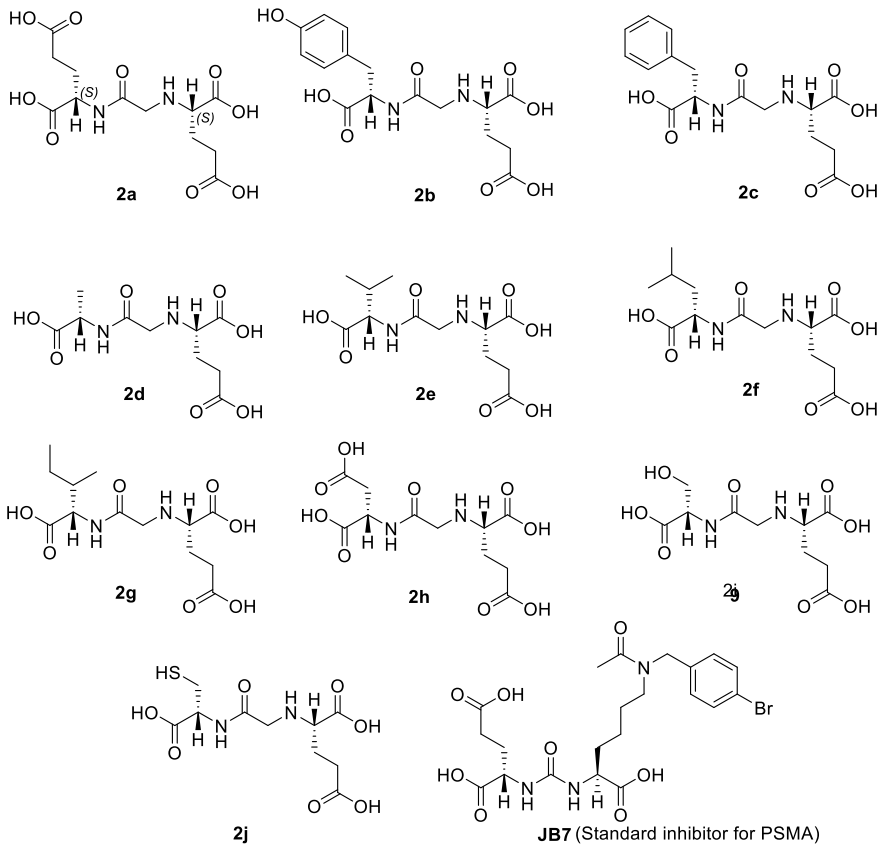

Figure 8. Designed aminoacetamide ligands **2a-j**

1.9.1 Proposed synthesis of protected aminoacetamide ligands

The *t*-butylcarboxy-protected amino acids **4a-j** can react with α-bromoacetic acid in presence of DCC and HOBt to provide α-bromoacetamide amino acids **3a-j**. The intermediate **3a-j** can be reacted with γ-benzylcarboxy-α-*t*-butylcarboxy glutamic acid in the presence of triethylamine (TEA) at 85 °C to afford tris(*t*-butylcarboxy)-γ-benzylcarboxy protected precursors **1a-j** (Scheme 2).

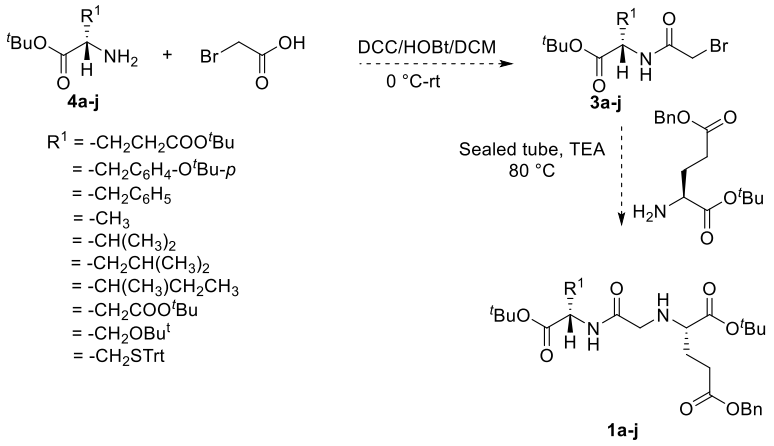

Scheme 2. Proposed synthesis of carboxy protected aminoacetamide precursors **1a-j**

1.9.2 Proposed synthesis of designed aminoacetamide ligands

The tris(*t*-butylcarboxy)-γ-benzylcarboxy protected precursors **1a-j** can be debenzylated by hydrogenation using palladium on charcoal to give debenzylated precursors **6a-j** which can be completely deprotected using mild trifluoroacetic acid in DCM solvent at room temperature to provide aminoacetamide ligands **2a-j** (Scheme 3).

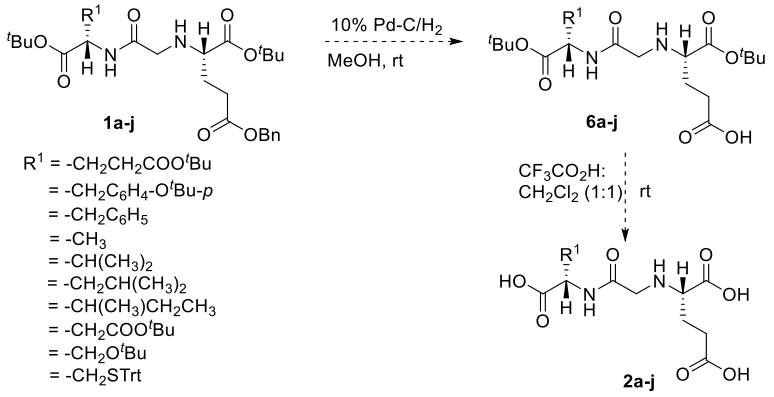

Scheme 3. Proposed deprotection to aminoacetamide ligands **2a-j**

1.9.3 Proposed synthesis of conjugation of aminoacetamide ligands with rhodamine B

Commercially available 1,2-diaminoethyltrityl resin **7** (Scheme 4) will be utilized to synthesize rhodamine B bioconjugate by following the standard procedure developed by our research group. The free amino group present in **7** will be coupled with Fmoc-Asp(OtBu)-OH using PyBOP as an amide coupling agent to provide dipeptide chain **8**. The NHFmoc amino group in the growing dipeptide chain **8** will be deprotected using a solution of 20% piperidine in DMF. The Fmoc free amino group in **8** will be now coupled with Fmoc-Lys(Tfa)-OH and 8-aminocaprylic acid to provide tetrapeptide **9** with trifluoroacetyl protected ε-amino group of lysine. It is important to mention that the α-amino group of lysine will be protected as NHFmoc which is labile to 20% piperidine in DMF and readily available for constructing next amide bond in the growing dipeptide chain. Whereas the ε-amino group of lysine protected as trifluoroacetyl group is stable under NHFmoc cleavage conditions and it readily undergoes deprotection in 2M aqueous piperidine. The selection of α- and ε-amine protecting groups in lysine amino acid, which are labile under different basic conditions, will be crucial to strategize the synthesis of attaching the fluorescent agent to ε-amino group of lysine in the final step of the preparation of conjugate **13**. After the deprotection of NHFmoc group, the tetrapeptide **9** will be tethered sequentially with two phenylalanine residues, another 8-aminocaprylic acid and finally to tris(*tert*-butoxy) AAPT precursor to afford the polypeptide chain **12**. The trifluoroacetyl group in lysine amino acid of polypeptide chain **12** will be deprotected using 2M aqueous piperidine and a fluorescent agent, rhodamine B will be coupled to lysine amino using PyBOP as coupling agent to give *tert*-butyl protected precursor of final conjugate **13**. Finally, the polypeptide chain **13** will be cleaved from the resin beads with the help of cleaving cocktail TFA:TIS:H_2O (95:2.5:2.5) solution to afford rhodamine B bioconjugate **13**.

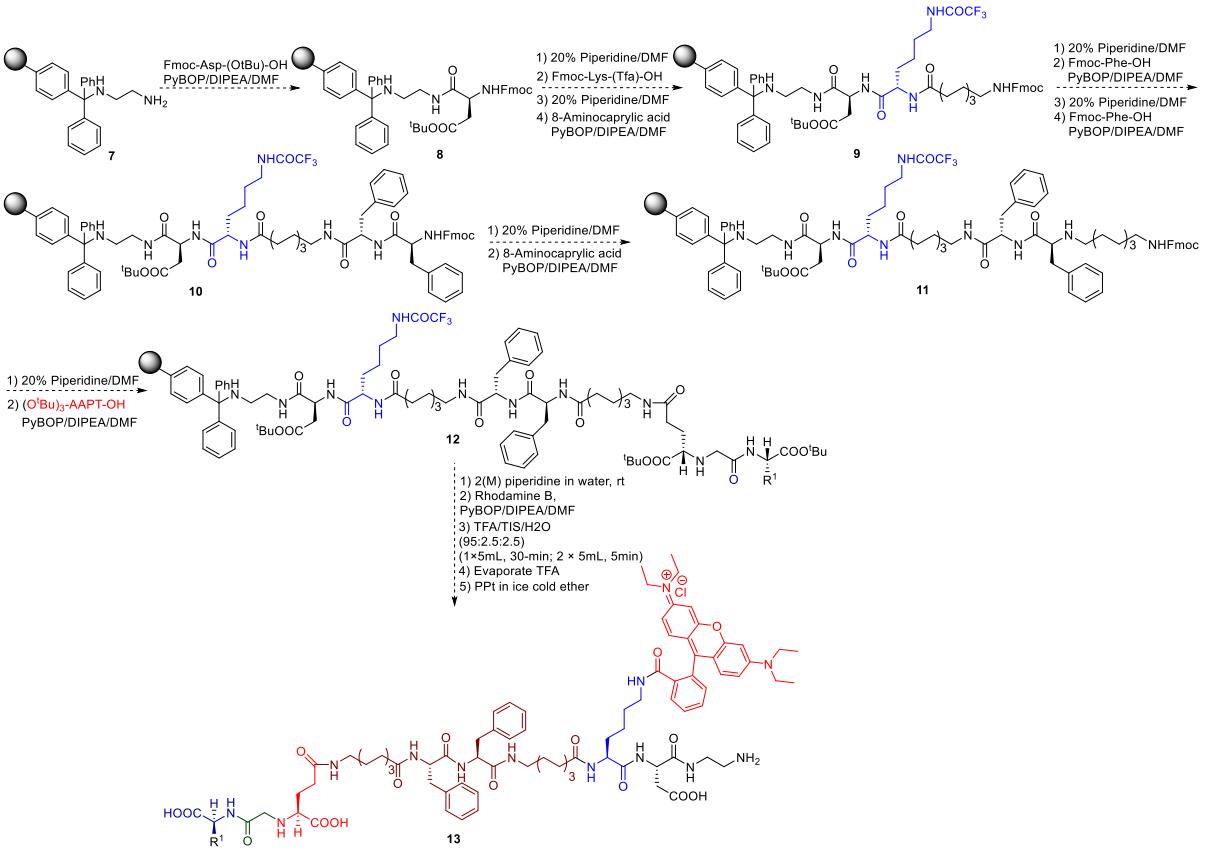

Scheme 4. Proposed SPPS for synthesis of rhodamine B bioconjugate **13** with aminoacetamide ligand

1.9.4 Proposed synthesis of chelating linker with glutamic acid-based aminoacetamide

The synthesis of chelating linker conjugate **21** will begin from commercially available 2-chlorotrityl cysteine resin **14** pre-attached to cysteine amino acid via carboxylic acid functional group (Scheme 5). The free amino group present in **14** will be subsequently coupled with Fmoc-Asp(O^{t}Bu)-OH, Boc-Dap(Fmoc)-OH to form the chelating core of **20**. The chelating core can be used as a multipurpose handle for loading drug cargos, radionuclides, or nanomaterials. Other amino acids like 8-aminocaprylic acid, phenylalanine, 4-(Fmoc-aminomethyl)benzoic acid will be utilized for the construction of **20** and the targeting ligand precursor tris(*tert*-butylcarboxy) AAPT will be attached to the peptide sequence in a similar fashion as described earlier for the construction of bioconjugate **13**. The polypeptide chain **19** will be detached from the chlorotrityl resin after attaching the targeting ligand and simultaneously all the carboxylic acid

protecting tert-butyl groups of amino acids will be deprotected with the help of cleavage cocktail TFA:EDT:TIPS:H_2O (92.5:2.5:2.5:2.5) to provide **20**.

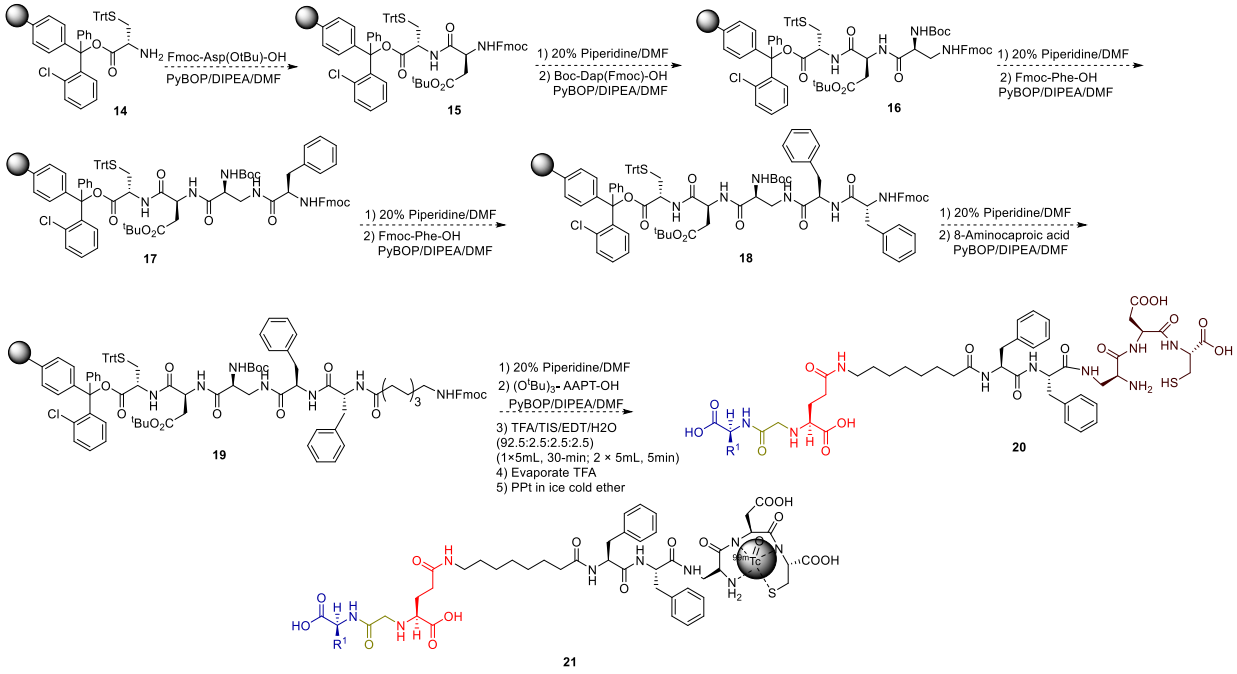

Scheme 5. Proposed synthesis of chelating bioconjugate **21** to deliver radio nuclide ^{99m}Tc

Chapter 2

LITERATURE REVIEW

2.1 Aminoacetamides as small molecule ligands

Being inspired by the substrate NAAG for PSMA, new small molecule ligands are designed. In 1996, it was reported that 2-PMPA (2-phosphonomethylpentanedioic acid) has the highest binding affinity (K_i = 0.275 nM) for PSMA protein [17]. Later, several urea-based small molecule ligands were designed and utilized for delivery of radioisotopes [18, 19].

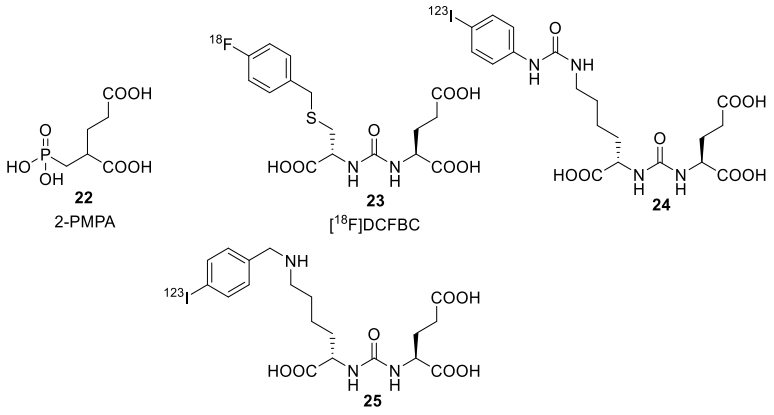

Figure 9. Urea based small molecule ligands for PSMA

It was also found that the ligands with S-amino acid configuration are more active than the ligands with R-configuration [20]. We have also recently synthesized aninoacetamide based PSMA small molecule ligands wherein the methylene carbon and amide moieties are switched between amino acids to afford different kind of PSMA ligands that are patented and currently in preclinical trials (Figure 10).

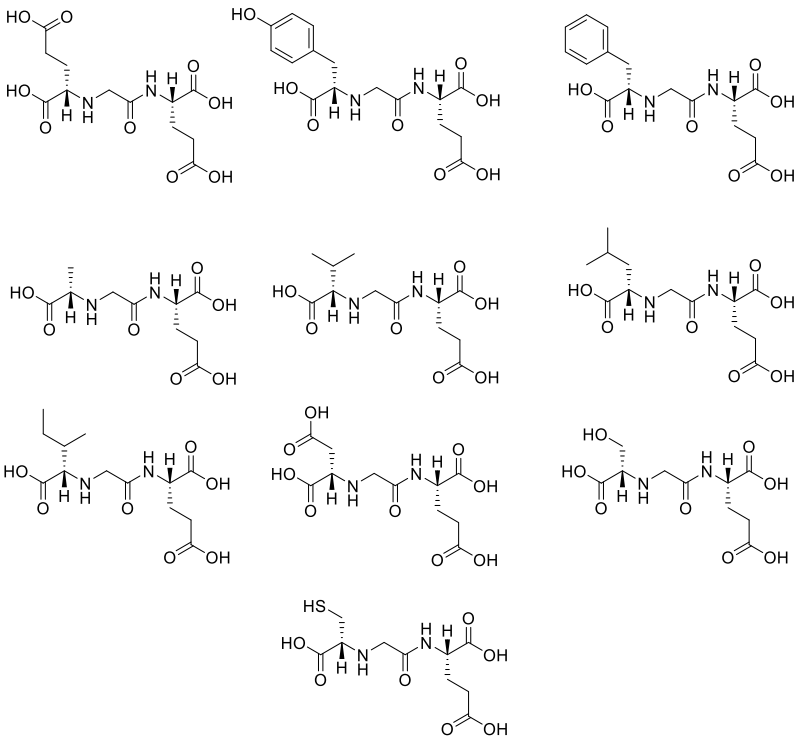

Figure 10. Aminoacetamide ligands for targeting PSMA with different structure

2.2 Molecular imaging probes for PSMA

The small molecule ligands are attached with fluorophore or radioisotopes with the help of linker which is made of amino acid residues. These conjugates can be used as molecular imaging probes for diagnosis of PCa (Figure 11). The conjugates with rhodamine B or IRDye800CW-NHS emits fluorescence in the range of near infrared (NIR) region [21-23].

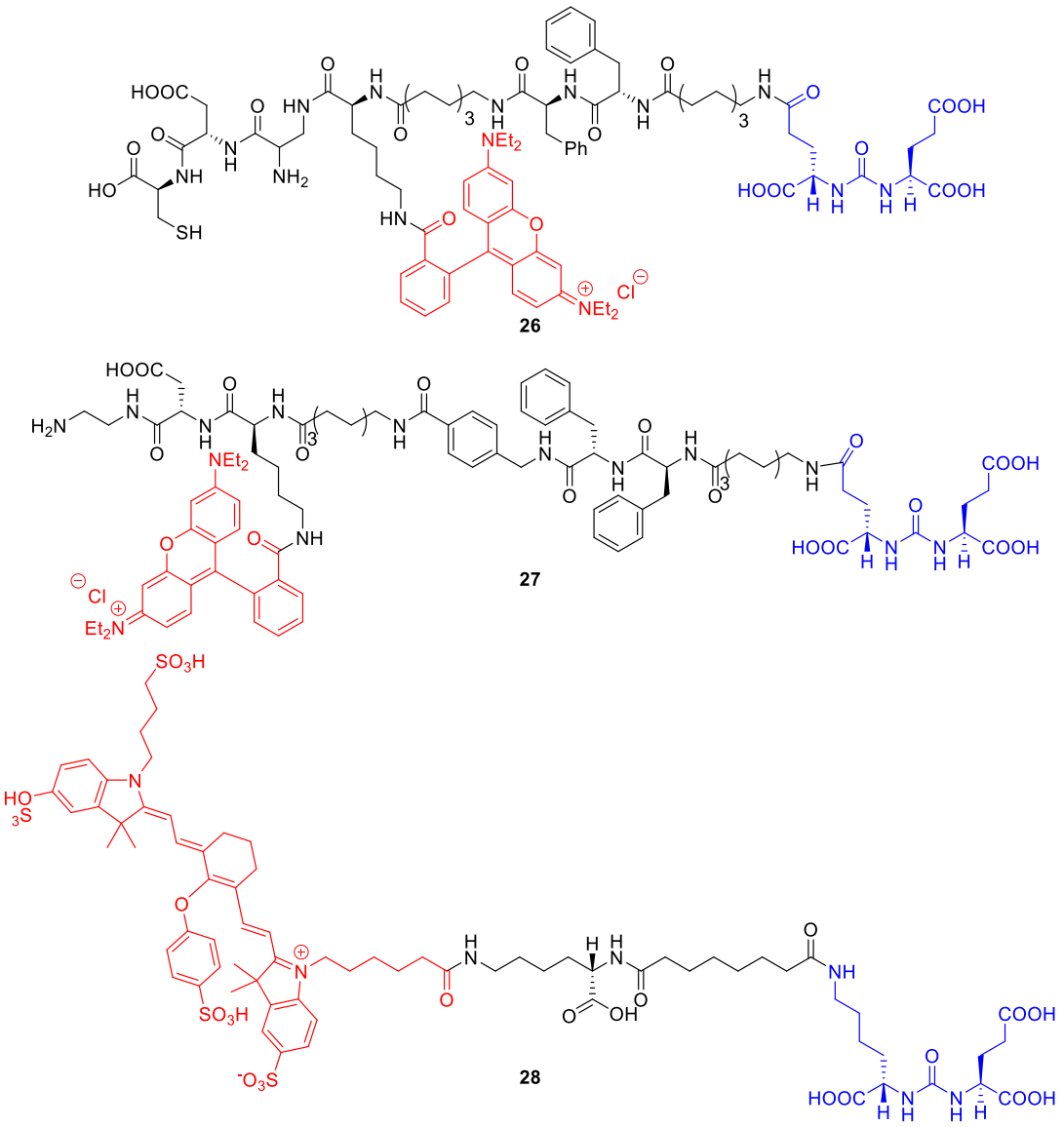

Figure 11. Molecular imaging probes for PCa

NIR quantum dots, QD655 [24], radio nuclides such as ^{99m}Tc, ^{68}Ga, ^{64}Cu were also used for imaging purpose [25-27]. Recently we have also reported from our research group the interaction of PSMA targeted bioconjugate with rhodamine B as fluorophore as shown in figure 12 [28].

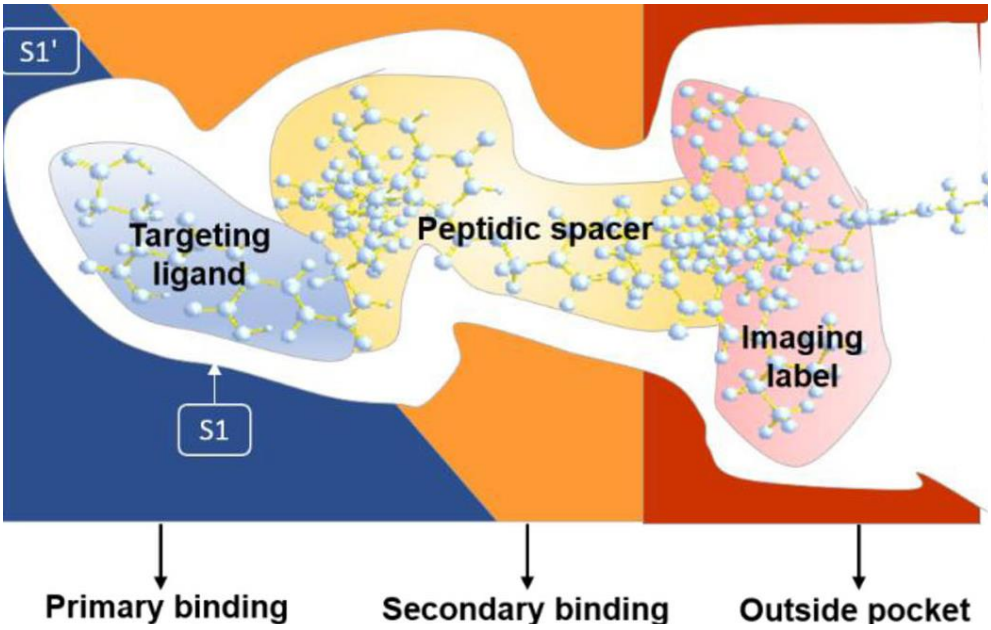

Figure 12. Interaction of imaging probe in PSMA [28]

Chapter 3

Experimental Section

3.1 General information

Amino acids, reagents, and solvents which were used in chemical synthesis, were purchased from Sigma-Aldrich, Merck, Iris Biotech GmbH, and Spectrochem. Drying agents like CaH_2, $CaCl_2$ were used to prepare anhydrous solvents by using standard procedures. Moisture-sensitive reactions were done under an inert nitrogen atmospheric condition and glasswares were used by drying in oven. Silica gel glass Thin Layer Chromatographic (TLC) plates (60 F_{254}) were used to monitor the chemical reactions and the spots of products were identified under UV light, iodine chamber and ninhydrin (for free primary amine). Appropriate reduced pressure and about 40 °C were used in rotary evaporator to remove volatile solvents. Distilled n-hexane and distilled ethyl acetate were used as eluents to purify compounds in silica gel column chromatography (100-200 or 230-400 mesh).

3.2 Drying of solvents

Various common organic solvents employed for carrying out reactions were dried using drying agents such as CaH_2, P_2O_5, $MgSO_4$ and Na_2SO_4.

3.2.1 Drying of DMF

DMF (50 mL) was taken in a round bottom flask (100 mL). A pinch of CaH_2 was added to the same flask with small spatula and was stirred overnight. Finally, the solvent was distilled off via vacuum distillation under reflux conditions and collected in another round bottom flask containing flame dried 4Å molecular sieves.

3.2.2 Drying of DCM

DCM (50 mL) was taken in a round bottom flask (100 mL). A pinch of CaH_2 was added to the same flask with a small spatula and was stirred overnight. Finally, the solvent was distilled off under reflux conditions and collected in another round bottom flask containing flame dried 4Å molecular sieves.

3.3 Protein preparation, Receptor grid generation and Molecular modelling studies to design new ligands

Molecular docking simulation based on extra-precision (XP) docking approach was performed on newly designed ligands (figure 8) on the PSMA ligand binding site for a better understanding of the binding mode of interaction between protein-ligands

complex by using the Schrodinger software suite. Build panel of the software was used to sketch the molecules in a 3D format which were further prepared for docking using LigPrep application. Co-crystallized protein complexed with ligand (JB7) was downloaded from Protein data bank (PDB ID: 4NGM) for docking study and optimized by using "Protein preparation wizard" which includes addition of hydrogen atoms, correction in bond orders, correction in missing residue side chain, deletion of water molecules and formation of disulfide bonds. Epik was used to generate heterogeneous states and Protassign was used for further optimisation of hydrogen bonds. Impref software was used to minimise the receptor energy at RMSD 0.30 by using force fields OPLS 2005. All the docking calculations were performed after generation of the grid around an active catalytic site of a protein receptor using receptor grid generation module of **Glide version 5.5.**

3.4 Synthesis of (S)-5-(tert-butoxy)-4-((2-(((S)-1,5-di-tert-butoxy-1,5-dioxopentan-2-yl)amino)-2-oxoethyl)amino)-5-oxopentanoic acid (6a)

3.4.1 Synthesis of di-*tertiary*-butyl L-glutamate from L-glutamic acid 4a

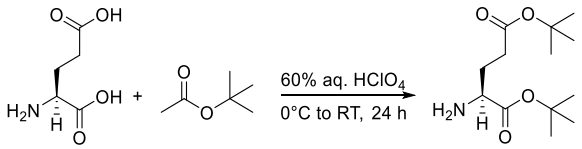

4a, 20 %

L-Glutamic acid (5 g, 33.98 mmol) was added to a single neck round bottom flask (250 mL). *Tertiary*-butyl acetate (100 mL, 747.56 mmol) was added using a measuring cylinder in one lot. The mixture was cooled to 0 °C and 60% perchloric acid (11.15 mL, 101.94 mmol) was added dropwise to the reaction mixture with stirring. The reaction mixture was warmed to room temperature and stirred for a further 26 h. After this, 0.5 N HCl (2 × 50 mL) was added to the reaction mixture and stirred for a few minutes. The aqueous layer was then separated and neutralized using solid Na_2CO_3. The aqueous layer was extracted with ethyl acetate (3 × 30 mL), washed with brine solution (25 mL), dried over anhydrous Na_2SO_4, filtered and the solvent evaporated using a rotary evaporator under reduced pressure to afford the crude mixture. The crude mixture was purified by column chromatography using 230-400 mesh silica with 30-90% ethyl acetate in hexane as eluent to afford di-*tertiary*-butyl L-glutamate. Yield

20% (1.8 g); R_f 0.5 (ethyl acetate). ^{1}H NMR (500 MHz, $CDCl_3$) δ 6.44 (s, 3H), 4.20 (t, 1H), 2.52 (t, 2H), 2.36 – 2.17 (m, 2H), 1.51 (s, 9H), 1.44 (s, 9H); ^{13}C NMR (125 MHz, $CDCl_3$) δ 173.07, 167.47, 85.29, 82.30, 53.62, 31.25, 28.01, 27.88, 25.17. MS (ESI) m/z $(M+H)^+$ calculated for $C_{13}H_{25}NO_4$: 260.1856; Observed: 260.1810.

3.4.2 Synthesis of 5-benzyl 1-(*tertiary*-butyl) L-glutamate 5

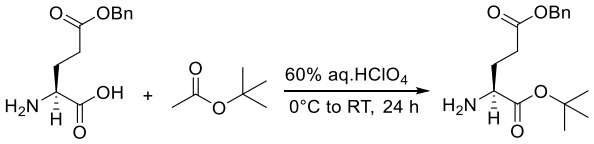

5-Benzyl glutamate (1 g, 4.21 mmol) was added to a single neck round bottom flask (50 mL). *Tertiary*-butyl acetate (20 mL) was added and cooled to 0 °C. 60% Aq. perchloric acid (1 mL) was added dropwise to the reaction mixture with stirring. The reaction mixture was warmed to room temperature and stirred for a further 24 h. 0.5 N HCl (8 × 10 mL) was added to the reaction mixture to extract the product. The aqueous layer was then separated and neutralized with solid Na_2CO_3 to pH 7-8. The aqueous layer was extracted with ethyl acetate (3 × 20 mL), washed with brine solution (25 mL), dried over anhydrous Na_2SO_4, filtered and the solvent evaporated using a rotary evaporator under reduced pressure to afford the crude mixture. The crude mixture was purified by column chromatography using 230-400 mesh silica gel with 30-80% ethyl acetate in hexane as eluent to afford 5-benzyl 1-(tertiary-butyl) L-glutamate. Yield 42% (0.520 g); R_f 0.5 (ethyl acetate). ^{1}H NMR (500 MHz, $CDCl_3$) δ 7.38–7.28 (m, 5H), 5.11 (s, 2H), 4.13 (dd, *J* = 8.7, 5.5 Hz, 1H), 3.71 (s, 1H), 2.60 (m, 2H), 2.27–2.14 (m, 1H), 2.08 (m, 1H), 1.46 (s, 9H).

3.4.3 Synthesis of α-bromoacetamido di-*tertiary* butylcarboxy glutamic ester 3a

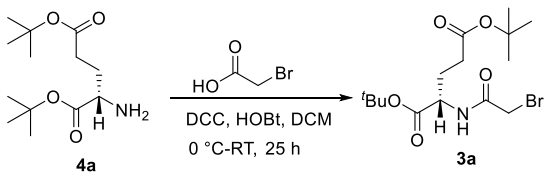

α-Bromoacetic acid (0.523 g, 3.76 mmol), HOBt (0.373 g, 2.757 mmol) and DCC (1.034 g, 5.012 mmol) were taken in a single neck RB (100 mL). Dry DCM (13 mL) was added to dissolve it under nitrogen atmosphere and stirred for 30 min. Di-*tert*-butyl glutamate (0.65 g, 2.506 mmol) was added to it as solution in dry DCM (7 mL). The reaction mixture was warmed to room temperature and continued stirring for 25 h. DCM was evaporated and ethyl acetate (13mL) was added to the residue. The white precipitate was filtered using Whatmann filter paper and the filtrate was concentrated to afford crude reaction mixture. The crude product was purified by column chromatography using 100-200 mesh silica gel with 0-8% ethyl acetate in hexane as eluent. Yield 57% (0.538 g); R_f 0.4 (1:3 ethyl acetate:hexane). ^{1}H NMR (500 MHz, $CDCl_3$) δ 7.09 (d, *J* = 7.7 Hz, 1H), 4.40 (td, *J* = 7.8, 4.9 Hz, 1H), 3.83 (s, 2H), 2.27 (m, 1H), 2.19 (m, 1H), 2.10 (m, 1H), 1.90 (m, 1H), 1.42 (s, 9H), 1.38 (s, 9H); ^{13}C NMR (125 MHz, $CDCl_3$) δ 172.12, 170.44, 165.75, 82.92, 52.97, 31.32, 28.72, 28.08, 27.99, 27.38, 25.47. MS (ESI) m/z $(M+Na)^+$ calculated for $C_{15}H_{26}BrNO_5$: 402.0887; Observed: 402.0896.

3.4.4 Synthesis of di-*tertiary*-butyl (2-chloroacetyl)-L-glutamate 3a'

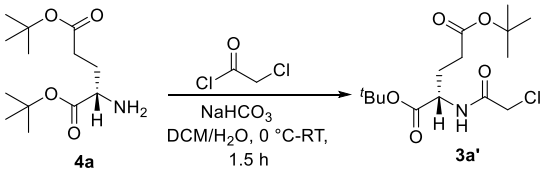

A stirred solution of di-^{t}butyl glutamate (1 g, 3.856 mmol) and sodium bicarbonate (0.809 g, 9.639 mmol) in DCM (5 mL, 5V) and water (0.5 mL, 0.5 V) was cooled to 0 °C. α-Chloroacetyl chloride (0.767 mL, 9.639 mmol) was added dropwise over a period of 15 minutes at 0 °C. The reaction mixture was stirred further for 1.5 h while the reaction warm to room temperature. The reaction mixture was diluted with water (15 mL) and DCM (10 mL). The organic layer was separated and washed with saturated sodium bicarbonate solution (2 × 20 mL). The organic layer was dried over anhydrous sodium sulphate and the crude product was purified by column chromatography using 100-200 mesh silica gel with 7-18% ethyl acetate in hexane as eluent to afford pure **3a'**. Yield 70% (0.905 g); R_f 0.6 (1:2 ethyl acetate:hexane). ^{1}H NMR (500 MHz, $CDCl_3$) δ 7.15 (d, *J* = 7.8 Hz, 1H), 4.43 (td, *J* = 7.9, 4.9 Hz, 1H), 3.99 (s, 2H), 2.32–2.23 (m, 1H), 2.19 (m, 1H), 2.15–2.05 (m, 1H), 1.90 (m, 1H), 1.42 (s, 9H), 1.38 (s, 9H); ^{13}C

NMR (125 MHz, $CDCl_3$) δ 170.97, 169.40, 164.90, 81.73, 79.84, 51.59, 41.43, 30.32, 27.05, 26.96, 26.39. HRMS (ESI) m/z $(M+Na)^+$ calculated for $C_{15}H_{26}ClNO_5$: 358.1392; Observed: 358.1395.

3.4.5 Synthesis of glutamic acid-based tris(*tertiary*-butylcarboxy) 1-benzylcarboxy aminoacetamide precursor 1a

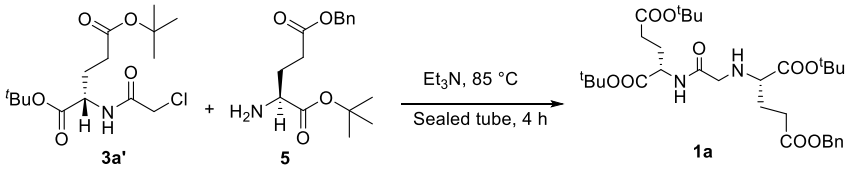

Di-*tertiary*-butyl (2-chloroacetyl)-L-glutamate **3a'** (0.1 g, 0.298 mmol) and 5-benzylcarboxy-1-*tertiary*-butylcarboxy glutamate **5** (0.087 g, 0.298 mmol) were dissolved in triethylamine (0.125 mL, 0.894 mmol) in a sealed tube and the reaction mixture was heated to 85 °C with stirring for 4 h. Ethyl acetate (15 mL) was added to the reaction mixture and the organic layer was washed with 0.5 N HCl (2 × 15 mL) followed by brine (20 mL) and dried over anhydrous sodium sulphate. The organic layer was concentrated under reduced pressure and crude product was purified by column chromatography over 100-200 mesh silica gel using 20-25% ethyl acetate in hexane as eluent to afford **1a**. Yield 21% (0.037 g); R_f 0.6 (1:1 ethyl acetate:hexane). ^{1}H NMR (500 MHz, $CDCl_3$) δ 7.60 (d, *J* = 8.5 Hz, 1H), 7.38 – 7.27 (m, 5H), 5.09 (d, *J* = 12.2 Hz, 1H), 5.16 (d, *J* = 12.2 Hz, 1H), 4.48 (td, *J* = 8.5, 5.0 Hz, 1H), 3.33 (d, *J* = 17.1 Hz, 1H), 3.10 (dd, *J* = 8.9, 5.1 Hz, 1H), 2.96 (d, *J* = 17.1 Hz, 1H), 2.65–2.49 (m, 2H), 2.35–2.21 (m, 2H), 2.17–2.09 (m, 1H), 2.06–1.97 (m, 1H), 1.96–1.84 (m, 3H), 1.43 (s, 9H), 1.43 (s, 9H), 1.44 (s, 9H); ^{13}C NMR (125 MHz, $CDCl_3$) δ 172.52, 172.10, 171.02, 170.12, 169.93, 134.89, 127.53, 127.37, 127.26, 125.97, 81.03, 80.93, 79.55, 65.33, 60.75, 50.68, 50.00, 30.68, 30.26, 28.68, 27.39, 27.07, 27.04, 26.98, 26.75. MS (ESI) m/z $(M+H)^+$ calculated for $C_{31}H_{48}N_2O_9$: 593.3224; Observed: 593.3433.

3.4.6 Synthesis of debenzylated tris(*tertiary*-butylcarboxy) AAPT precursor 6a

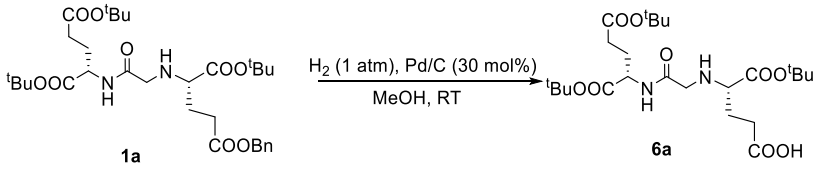

Tris(*tertiary*-butylcarboxy) 1-benzylcarboxy aminoacetamide precursor **1a** (0.500 g, 0.844 mmol) was taken in two neck RB (50 mL) and dissolved in methanol (15 mL). Slowly 10% Pd/C (0.269 g, 30% mol) was added to the reaction mixture and purged with H_2 gas in a bladder. The reaction mixture was further stirred for 45 h. After the completion of the reaction by TLC, the reaction mixture was filtered through a celite 545 pad taken in sintered Buchner funnel and filtered using a filtration pump. The celite pad was washed with methanol (3 × 15 mL). The filtrate was concentrated and purified by column chromatography using 100-200 mesh silica gel with 10-100% ethyl acetate in hexane as eluent.

Chapter 4

Results and Discussion

4.1. Design of new inhibitors

Inspired by the molecular structure of endogenous PSMA substrates such as NAAG and folyl-γ-Glu, at the S1 pocket of PSMA, a methylene carbon unit has been inserted between carbonyl carbon and nitrogen of amide bond, in the newly designed inhibitors, to enhance the number of new interactions in the binding pocket of PSMA. Further L-glutamic acid-based aminoacetamide inhibitors **2a-j** (Figure 8), which closely resemble NAAG as well as folyl-γ-Glu, has been designed to examine the structural and functional requirements necessary for binding at the active site of the PSMA protein.

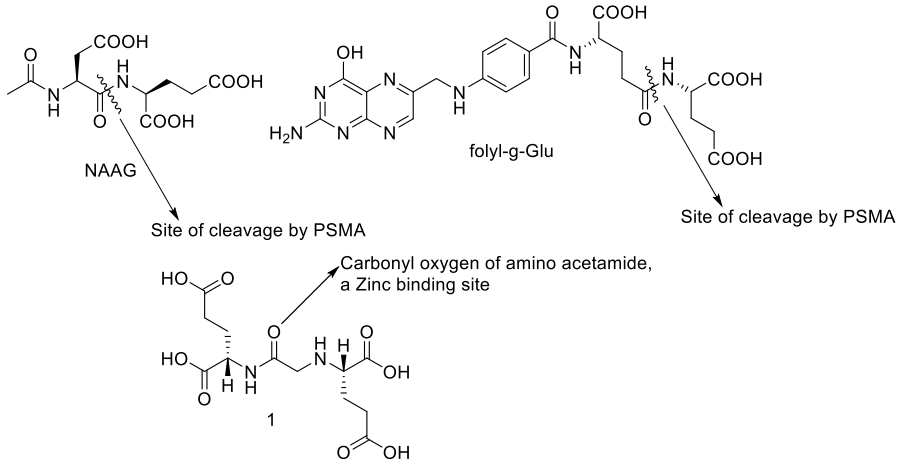

Figure 13. Design of lead aminoacetamide peptidomimetic **1** for PSMA enzyme inhibition

It is well documented that the active site of the GCPII protein contains hydrophobic (S1 pocket) and hydrophilic pocket (S1' pocket) and the interactions at the S1' site are believed to be more critical for better binding affinity. Literature report suggests that JB7 interact with several amino acid residues such as Tyr 700, Arg 210, Lys 699, Asn 257, Gly 518, Tyr 552, Glu 424, Asn 519, Arg 536, and Arg 534 through hydrogen bonds that are critical for better binding of a ligand with the protein. Therefore, the aforementioned amino acid interactions should be taken into consideration while performing docking studies of the newly designed ligands **1**–**10** with GCPII protein.

Table 2 shows a correlation between amino acid residues of S1 and S1' pockets present in PSMA protein and the newly designed amino-acetamide ligands **2a**–**j** interacting

through hydrogen bonds. In addition, some extra hydrogen bonding interaction with Val 208, Gly 548, Ser 547, Asn 544, Lys 539, Gly 548 and Glu 457 residues was also observed (Table 2).

Table 2. Hydrogen bonding interactions between GCPII protein and aminoacetamide ligands **2a-j** along with the bond distance of interaction in Å

Site	Amino acid residue	JB7 Post or re docking interactions with GCPII in Å	H-bonding interactions of ligands 1-10 with GCPII protein in Å									
			2a	**2b**	**2c**	**2d**	**5e**	**2f**	**2g**	**2h**	**2i**	**2j**
S1' site of GCPII (Hydrophilic pocket)	**Arg 210**	2.14			2.05	2.60		2.45	1.90		2.28	
	Asn 257										2.72	
	Lys 699	1.70										
	Tyr 552					1.90		1.99				
	Tyr 700	1.59			1.77	1.79		1.95	2.03		2.08	
	Glu 424		2.32	2.32	2.30	2.46	2.33	2.26	2.30	2.37	1.92	2.39
	Glu 425											
	Tyr 552		2.09	2.37	2.08		2.26		2.12	1.99		2.13
S1 site of GCPII (Hydrophobic pocket)	**Gly 518**	**1.79 2.08**				**1.97**		**1.94**	**1.99**			
	Asn 519	1.95	1.87				1.90			2.49	2.06	2.12
	Arg 534	1.82	1.66	1.65	2.71 2.68	1.92 2.33	1.76 2.79	2.51 2.20	2.77 2.26	1.78	1.92 2.15 2.70	1.72
	Arg 536	1.82		2.16	1.83	1.83	2.07	1.99	1.82	1.82	1.79	2.0
	Asp 453											
	Asp 387											
	Ser 454											
	Tyr 549											
	Ser 517										2.18	
	Arg 463		1.99		1.61	1.63		1.52	1.71		2.10	
Other Interactions	**Val 208**			**1.90**								
	Gly 548		**1.87**									
	Ser 547		**2.53**									
	Asn 544		**1.97**							**2.12**		
	Lys 539		**1.86**							**1.81**		
	Gly 548									**2.43**		
	Glu 457									**1.89**		

The exposure of three-dimensional crystal structures of PDB 4NGM complexed with inhibitor gives valuable insight into key interactions between ligand and enzyme. The binding free energy of the protein-ligand complex was calculated using the prime module. Moreover, in the glide module of the Schrodinger software suite, hydrogen bond distances more than 3 Å length are considered as weak and are not visible during docking study. Among the newly designed aminoacetamide ligands, the docking score of **2b** is found to be the highest followed by ligand **2a** (second most active) in the series. Brief information for docking results of NGM series is given in table 3.

Table 3. Molecular docking scores of aminoacetamide ligands **2a-j** and JB7 with GCPII protein (PDB 4NGM)

Rank	**Ligand**	**Docking score**
1	**2b**	-15.313
2	**2a**	-15.068
3	**JB7**	-15.004
4	**2h**	-14.649
5	**2c**	-14.321
6	**2i**	-14.122
7	**2f**	-13.697
8	**2g**	-13.605
9	**2d**	-13.061
10	**2j**	-12.132
11	**2e**	-11.323

The most active ligand, **2b**, in the series is oriented toward the residues of PSMA protein in such a way that it interacts extensively at the hydrophilic S1' pocket of the side chain of protein at the active site with Glu424, Tyr552, and Tyr700 residues through two hydrogen bonds and π-π stacking interactions, respectively, while JB7 interacts at same pocket through Arg210, Lys699, and Tyr700 with hydrogen-bonding

interactions. In the hydrophobic S1 pocket of the enzyme, ligand **2b** and JB7 show the same interactions where both are interacting with the same amino acid residues (Arg534 and Arg536 respectively) through carboxylic acid moiety present in the structure. Apart from these interactions, the most active ligand **2b** of the series forms an additional H-bond at the backbone of protein where the phenolic group of tyrosine moiety interacts with the carbonyl oxygen of Val208. This fact suggests that the tyrosine moiety of **2b** interacts strongly with the protein active site compared to JB7 (Figures 14 and 15). At the hydrophobic pocket of the active site of PSMA protein, the hydroxyl group of the glutamic acid moiety of ligand **2a** interacts with a free amino group of Arg534 with a bond length of 1.65 Å which is considerably less in comparison to the bonding length of JB7 which is 1.82 Å.

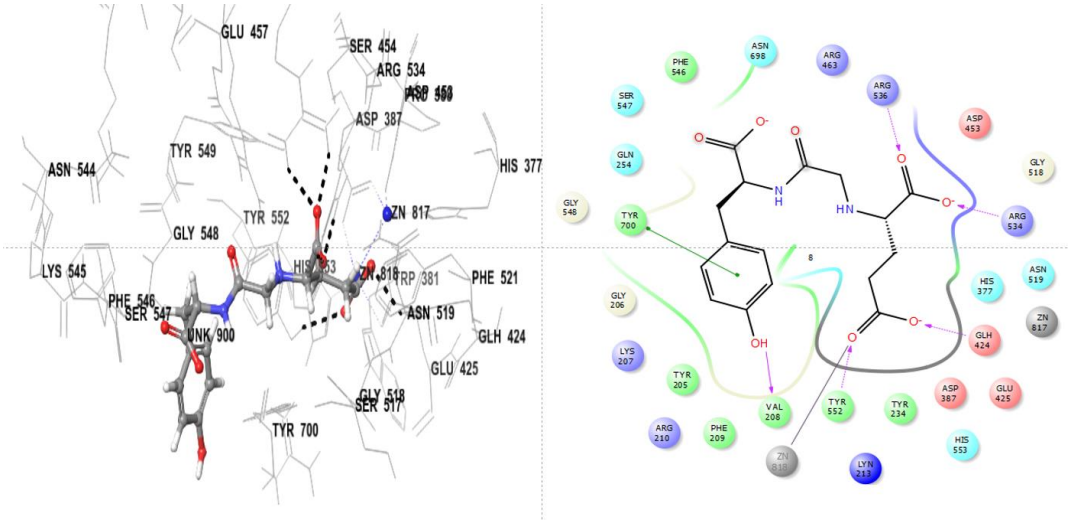

Figure 14. Molecular docking study of inhibitor **2b** at GCPII active cavity (PDB 4NGM)

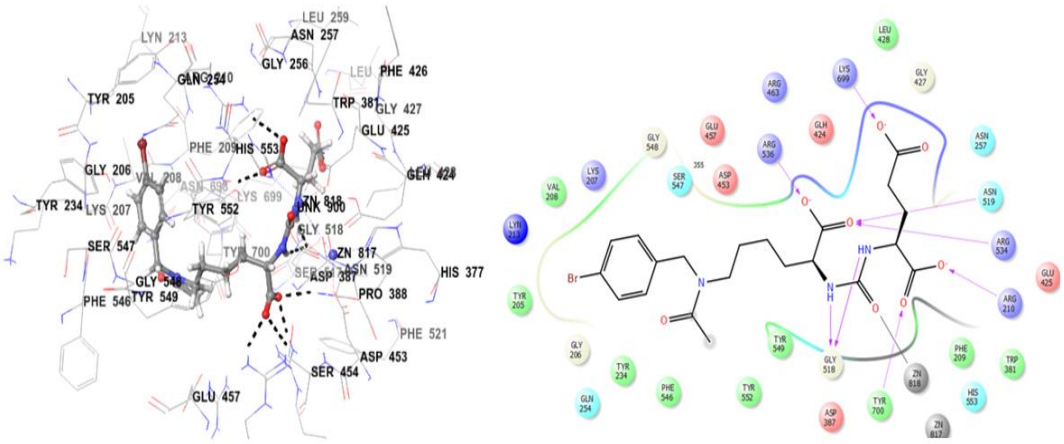

Figure 15. Molecular docking study of JB7 with GCPII protein (PDB 4NGM)

The ligand **2a** has also shown similar hydrogen bonding interactions as ligand **2b** towards the amino acid residues Glu424 and Tyr552 located at the side chain of S1' pocket of the active site of PSMA while π-π stacking interaction with Tyr700 is absent which may be a significant reason for slightly less activity of **2a** compared with ligand **2b**. Also, ligand **2a** shows one extra hydrogen bond with the sidechain of the hydrophobic pocket of the active site of protein where oxygen moiety of acetamido group of ligand interacts with guanidine moiety of Arg463. Apart from S1 and S1' pockets, ligand **2a** also shows hydrogen bonding interactions with Gly548, Ser547, Asn544, and Lys 539 residues, respectively which is due to the presence of polar glutamate scaffold in the molecular framework of the ligand **2a** (Figure 16).

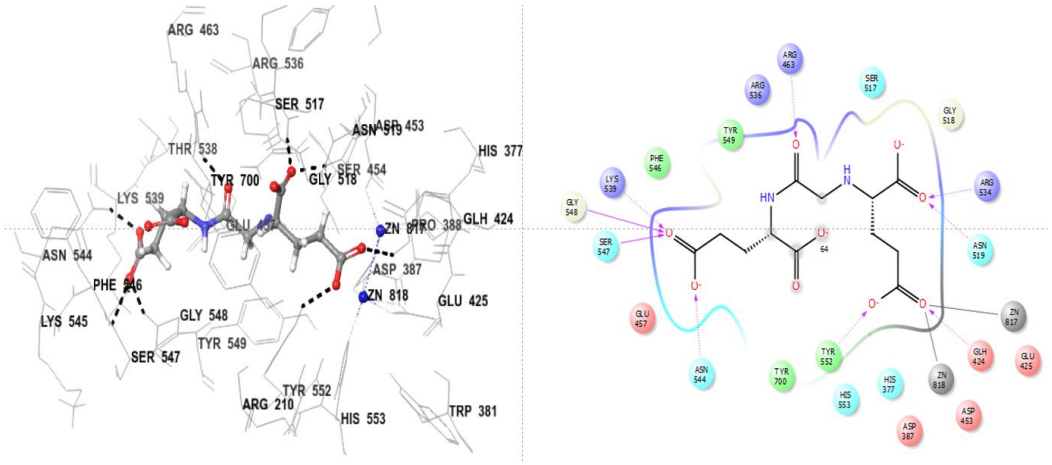

Figure 16. Molecular docking study of inhibitor **2a** at GCPII active cavity (PDB 4NGM)

Further, to analyze the effect of polar and non-polar substituents on the efficiency of ligands to inhibit the activity of the GCPII enzyme, several derivatives of 2-amino acetamide ligands have been designed and synthesized for evaluation. After tyrosine (**2b**) and glutamate (**2a)** ligands, the aspartic acid derivative (**2h**) was observed to have better docking scores compared to the other designed analogs.

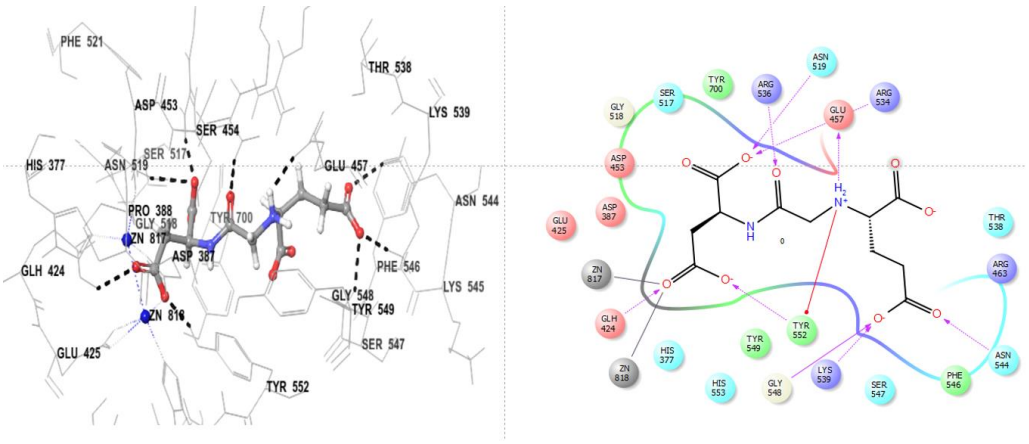

Figure 17. Molecular docking study of inhibitor **2h** at GCPII active cavity (PDB 4NGM)

4.2 Synthesis of glutamic acid-based aminoacetamide ligand (6a)

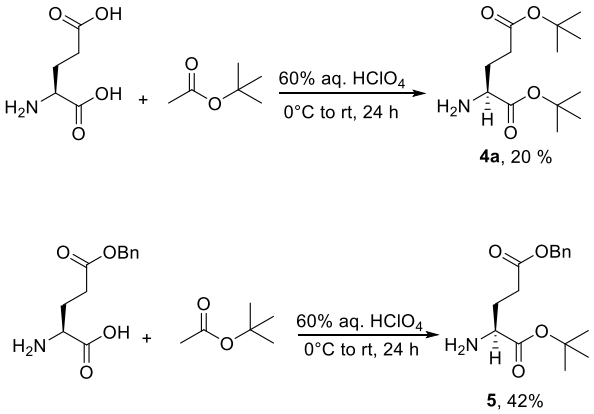

Scheme 6. Preparation of di-*tertiary*-butyl L-glutamate (**4a**) and 5-benzyl 1-(*tertiary*-butyl) L-glutamate (**5**)

With the retrosynthetic approach in our hand, synthesis of **2a** commenced with the preparation of *tertiary*-butylcarboxy protected amino esters **4a** and **5** (Scheme 6). The reaction of L-glutamic acid with *tertiary*-butyl acetate in the presence of an acidic medium provided di-*tertiary*-butyl L-glutamate **4a**. Whereas the reaction of 5-benzyl glutamate with *tert*-butyl acetate in an acidic medium afforded the corresponding 5-benzyl 1-(*tertiary*-butyl) L-glutamate **5**. Generation of *a tertiary*-butyl carbocation from *tertiary*-butyl acetate in acidic conditions furnished **4a** and **5** in 20% and 42% yields, respectively. The protected esters are sensitive to moisture, undergo considerable decomposition over time, and are therefore used as early as possible after their preparations without long-term storage.

Di-*tertiary*-butyl L-glutamate **4a** was coupled with α-bromoacetic acid using DCC as a coupling agent in the presence of HOBt to form activated hydroxybenzotriazole ester of α-bromoacetic acid which on reaction with **4a** afforded di-*tertiary*-butyl (2-bromoacetyl)-L-glutamate **3a** in 57% yield. However, our various attempts to displace bromide from **3a** using 5-benzyl 1-(*tertiary*-butyl) L-glutamate **5** were not successful to synthesize tris(*tertiary*-butylcarboxy) 1-benzylcarboxy aminoacetamide precursor **1a** (Scheme 7).

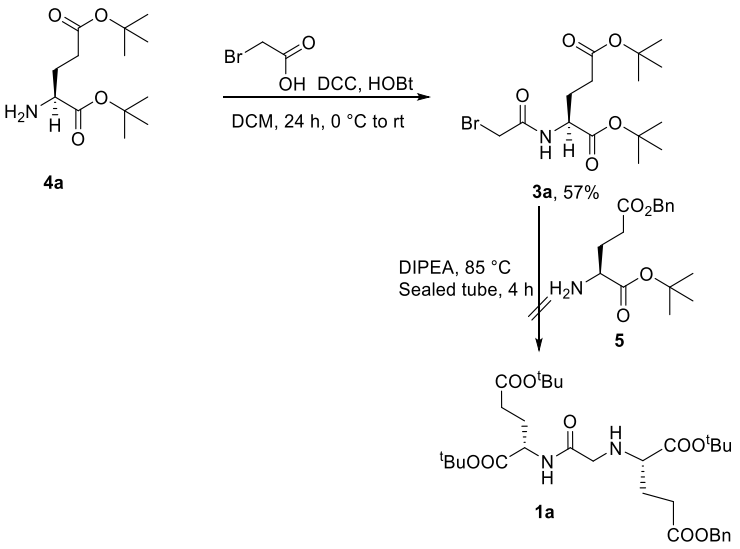

Scheme 7. Attempted preparation of tris(*tertiary*-butylcarboxy) 1-benzylcarboxy aminoacetamide precursor **1a** from **3a**

Next, we reacted **4a** with α-chloroacetyl chloride in a biphasic reaction using water and CH_2Cl_2 in presence of a mild base like $NaHCO_3$ to afford di-*tertiary*-butyl (2-chloroacetyl)-L-glutamate **3a'** in a higher yield of 70%. Finally, the chloride in **3a'** was displaced with 5-benzyl 1-(*tertiary*-butyl) L-glutamate **5** in presence of Et_3N as a base in a sealed tube at 85 ˚C to provide tris(*tertiary*-butylcarboxy) 1-benzylcarboxy aminoacetamide precursor **1a** albeit in a low yield of 21% (Scheme 8). The reaction conditions are currently under optimization to improve the yield of **1a**. Utilization of DIPEA as a base resulted in the formation of **1a** in 10% yield despite performing the reaction for a shorter time (4-18 h).

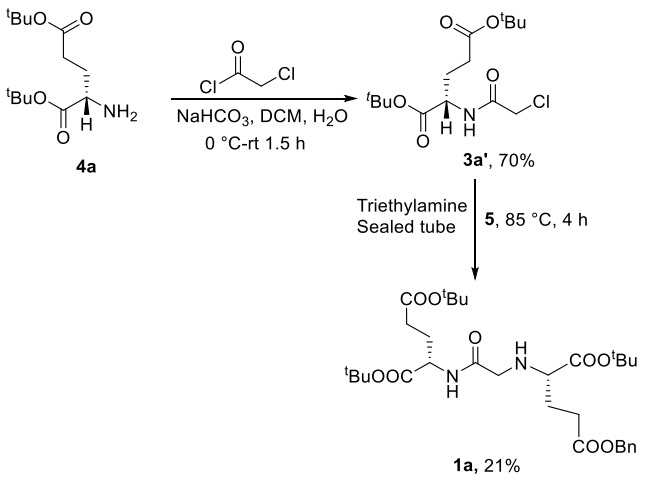

Scheme 8. Preparation of tris(*tertiary*-butylcarboxy) 1-benzylcarboxy aminoacetamide precursor **1a** from **3a'**

Debenzylation of **1a** in presence of H_2(1 atm)/Pd-C in MeOH at room temperature resulted in the formation of tris(*tertiary*-butylcarboxy) aminoacetamide glutamic acid precursor **6a** in poor yield and the reaction conditions are being optimized currently (Scheme 9). A carboxylic acid group is available, and it can be used as a handle to attach the peptide linker to provide the required bioconjugates.

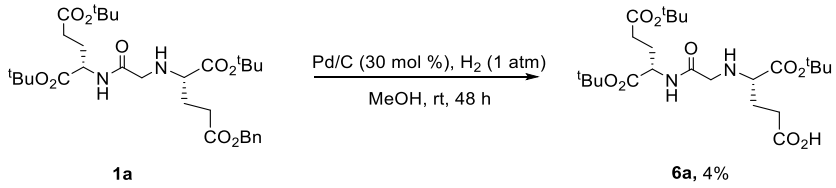

Scheme 9. Preparation of tris(*tertiary*-butylcarboxy) aminoacetamide glutamic acid precursor **6a**

4.3 Synthesis of conjugation of aminoacetamide ligands with rhodamine B

Commercially available 1,2-diaminoethyltrityl resin **7** (Scheme 4) was utilized to synthesize rhodamine B bioconjugate by following the procedure reported by our research group. The free amino group present in **7** was coupled with Fmoc-Asp(OtBu)-OH using PyBOP as an amide coupling agent to provide dipeptide chain **8**. The NHFmoc amino group in the growing dipeptide chain **8** was deprotected using a solution of 20% piperidine in DMF. The Fmoc free amino group in **8** was now coupled

with Fmoc-Lys(Tfa)-OH and 8-aminocaprylic acid to provide tetrapeptide **9** with trifluoroacetyl protected ε-amino group of lysine. It was important to mention that the α-amino group of lysine was protected as NHFmoc which is labile to 20% piperidine in DMF and readily available for constructing next amide bond in the growing dipeptide chain. Whereas the ε-amino group of lysine protected as trifluoroacetyl group is stable under NHFmoc cleavage conditions and it readily undergoes deprotection in 2M aqueous piperidine. The selection of α- and ε-amine protecting groups in lysine amino acid, which are labile under different basic conditions, was crucial to strategize the synthesis of attaching the fluorescent agent to ε-amino group of lysine in the final step of the preparation of conjugate **13**. After the deprotection of NHFmoc group, the tetrapeptide **9** was tethered sequentially with two phenylalanine residues, another 8-aminocaprylic acid, and finally to tris(*tert*-butoxy) AAPT precursor to afford the polypeptide chain **12**. The trifluoroacetyl group in lysine amino acid of polypeptide chain **12** was deprotected using 2M aqueous piperidine and a fluorescent agent, rhodamine B was coupled to lysine amino using PyBOP as a coupling agent to give *tert*-butyl protected precursor of final conjugate **13**. Finally, the polypeptide chain **13** was cleaved from the resin beads with the help of a cleaving cocktail TFA:TIS:H_2O (95:2.5:2.5) solution to afford rhodamine B bioconjugate **13**.

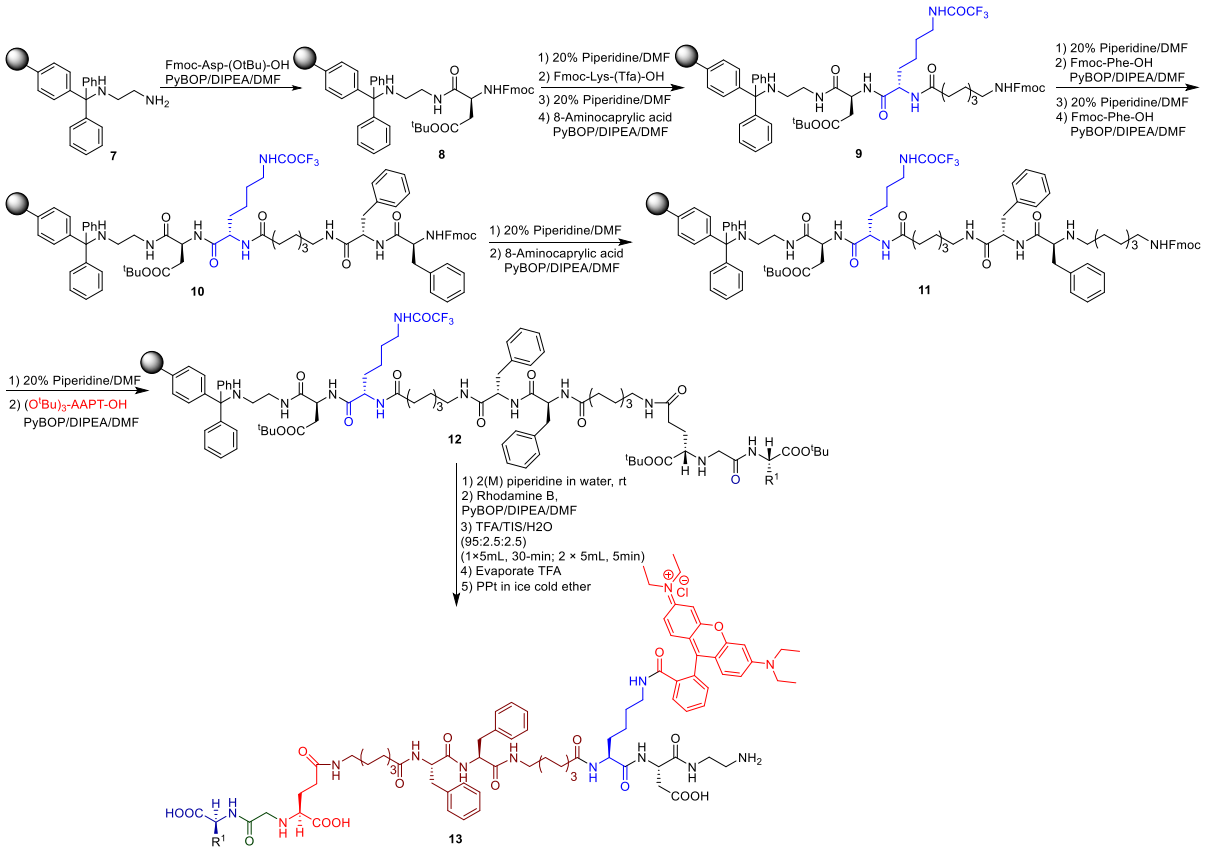

Scheme 10. SPPS for the synthesis of rhodamine B bioconjugate **13** with aminoacetamide ligand

Chapter 5

CONCLUSION

For imaging as well as for therapeutic applications selective delivery of cargo is important. We have designed targeting ligands with aminoacetamide core and plan to synthesize bioconjugates that can be used as a molecular imaging probe for the diagnosis of PCa in the future. Molecular docking studies are being performed to design targeting ligands with better binding affinity to PSMA protein. Currently, we are synthesizing the targeting ligands with various amino acids to confer hydrophilic or hydrophobic properties, and later we will perform in vitro enzyme inhibition analysis to identify high-affinity ligands that can be conjugated with fluorophores or radioisotopes to develop molecular imaging or therapeutic agents.

APPENDIX A

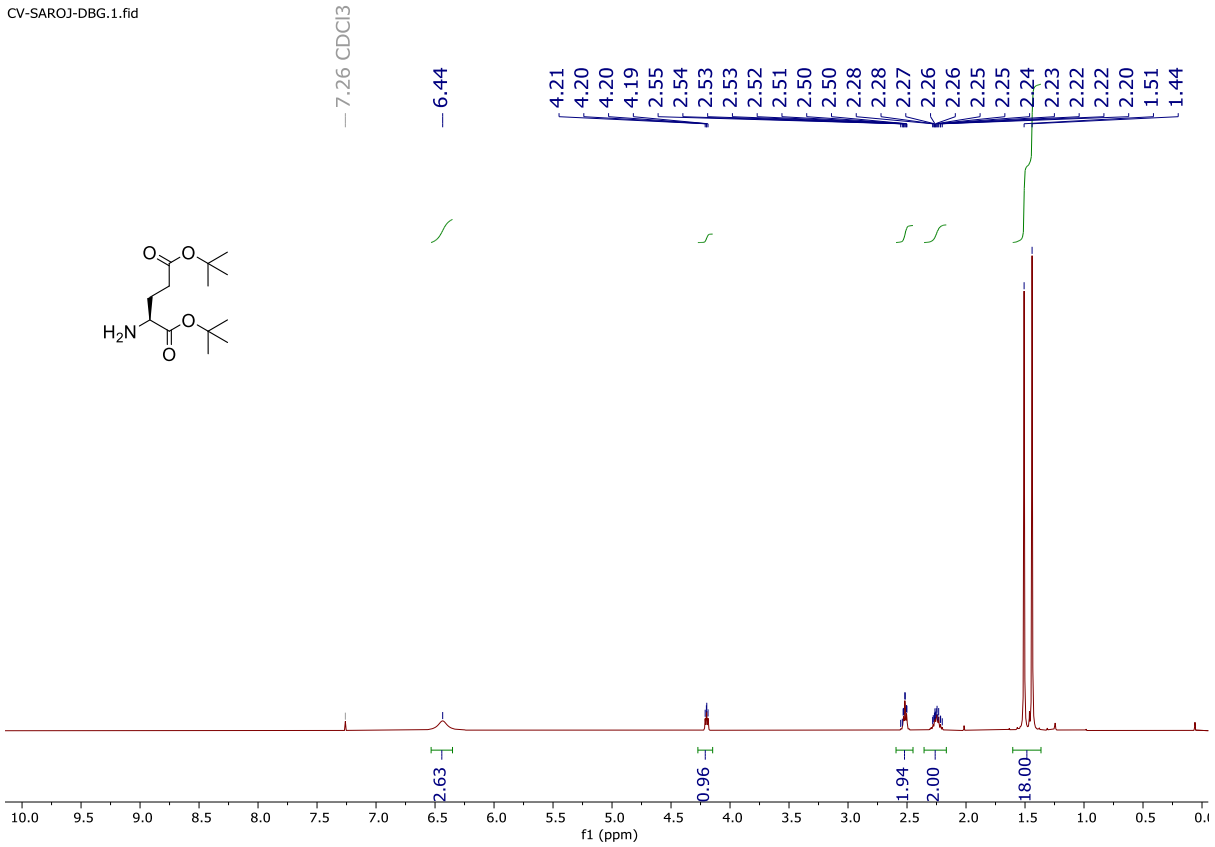

Figure 18. ^{1}H NMR spectrum (500 MHz) of **4a** in $CDCl_3$

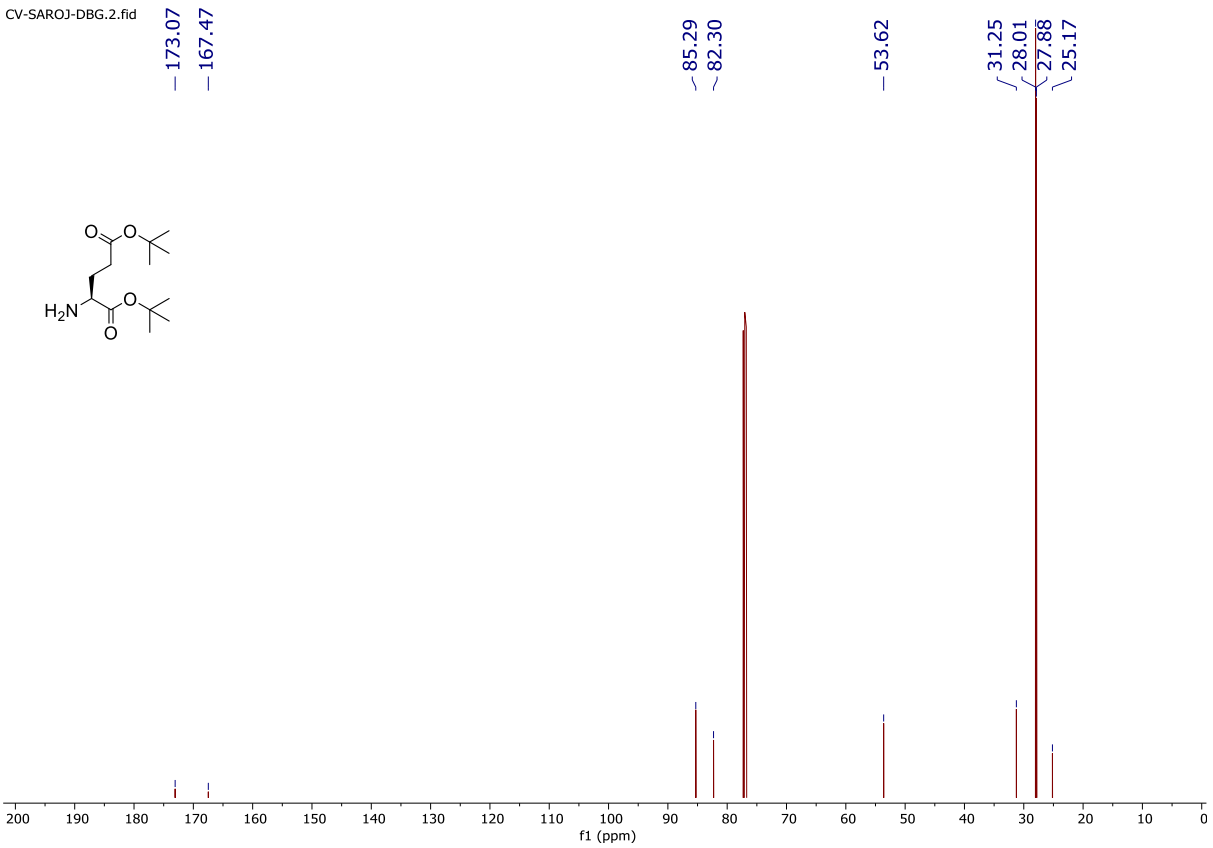

Figure 19. ^{13}C NMR spectrum (125 MHz) of **4a** in $CDCl_3$

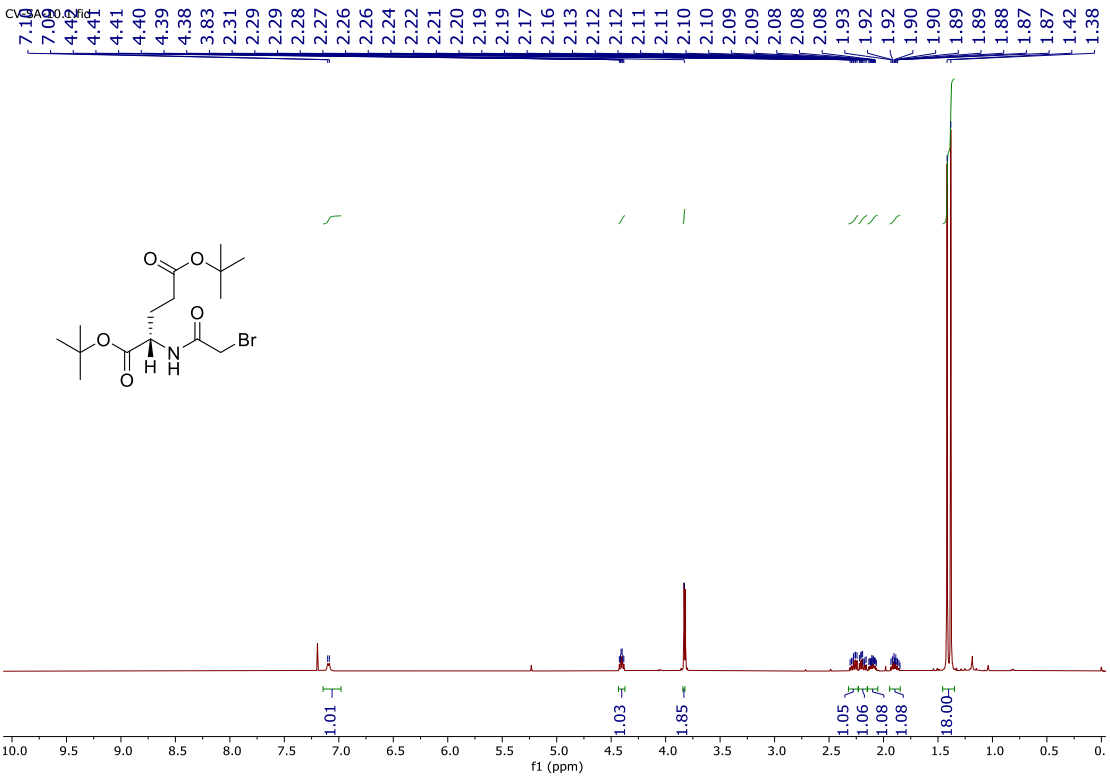

Figure 20. ^{1}H NMR spectrum (500 MHz) of **3a** in $CDCl_3$

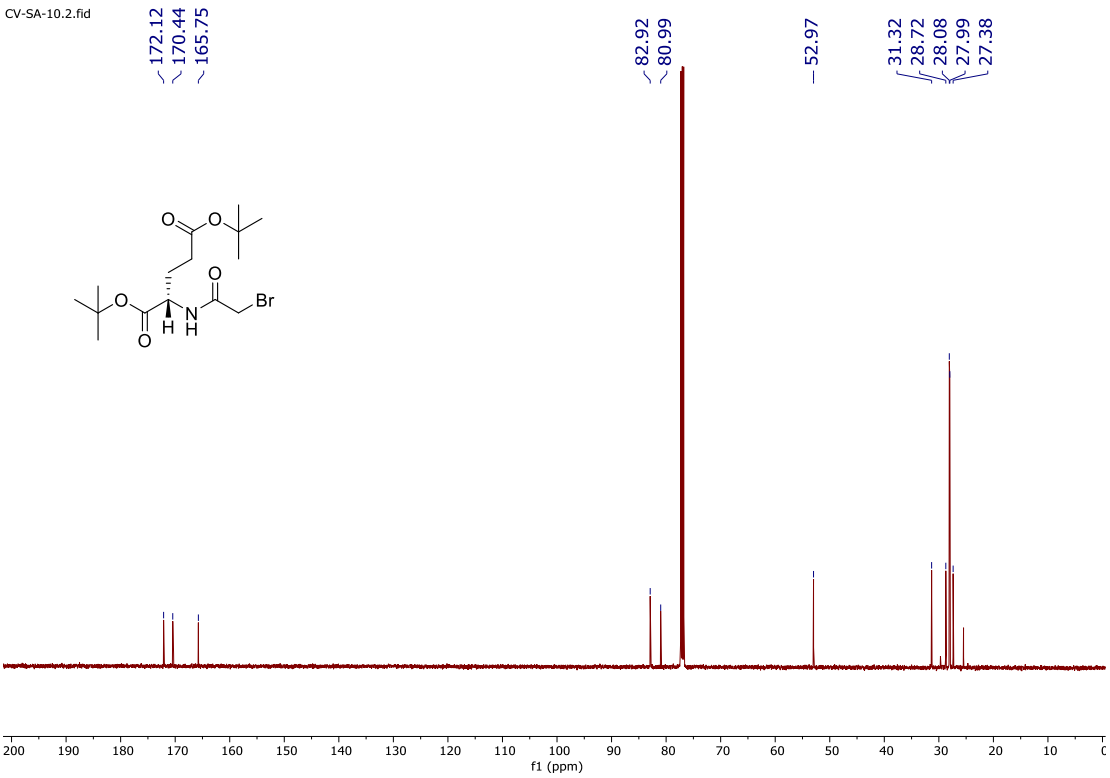

Figure 21. ^{13}C NMR spectrum (125 MHz) of **3a** in $CDCl_3$

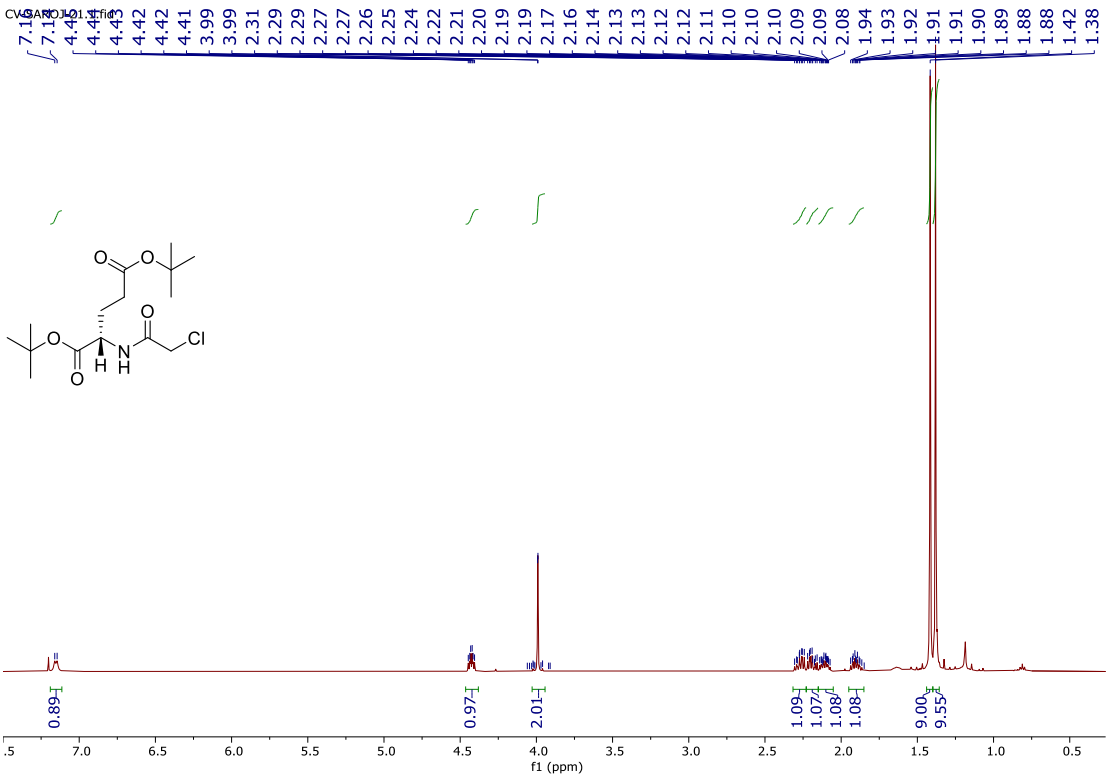

Figure 22. ^{1}H NMR spectrum (500 MHz) of **3a'** in $CDCl_3$

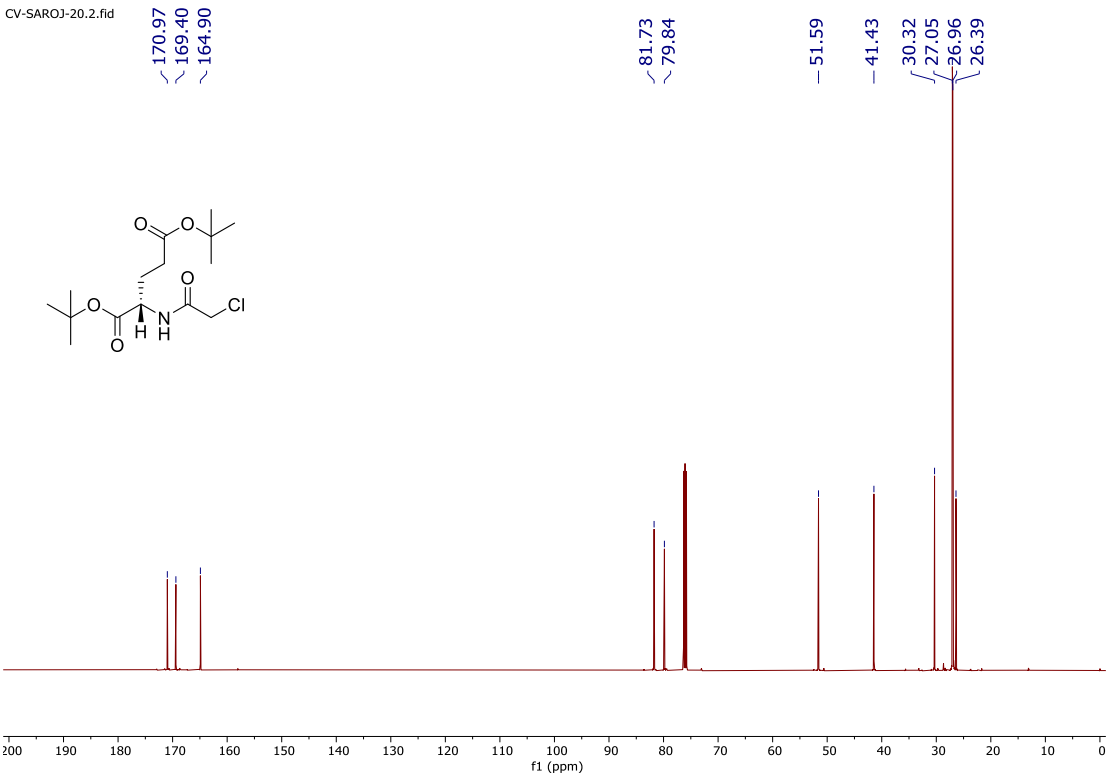

Figure 23. ^{13}C NMR spectrum (125 MHz) of **3a'** in $CDCl_3$

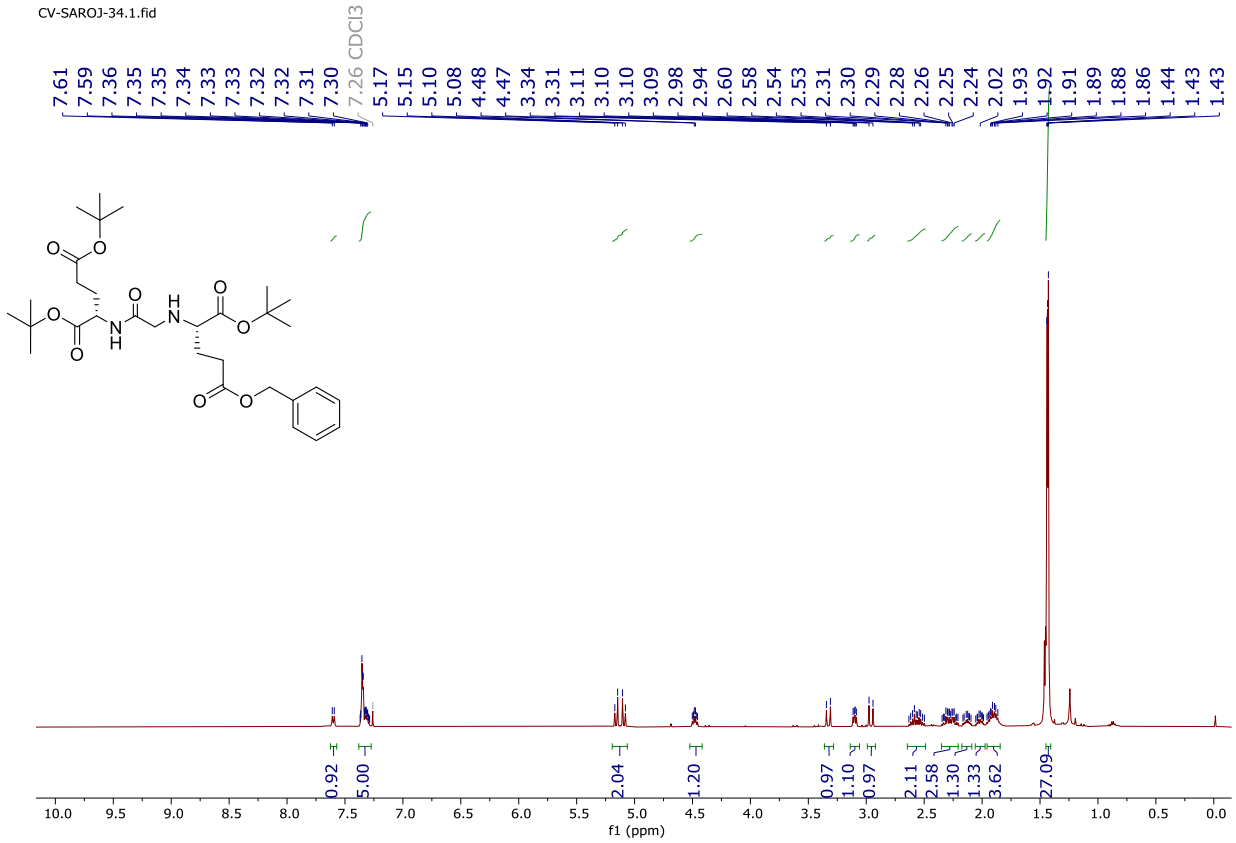

Figure 24. ^{1}H NMR spectrum (500 MHz) of **1a** in $CDCl_3$

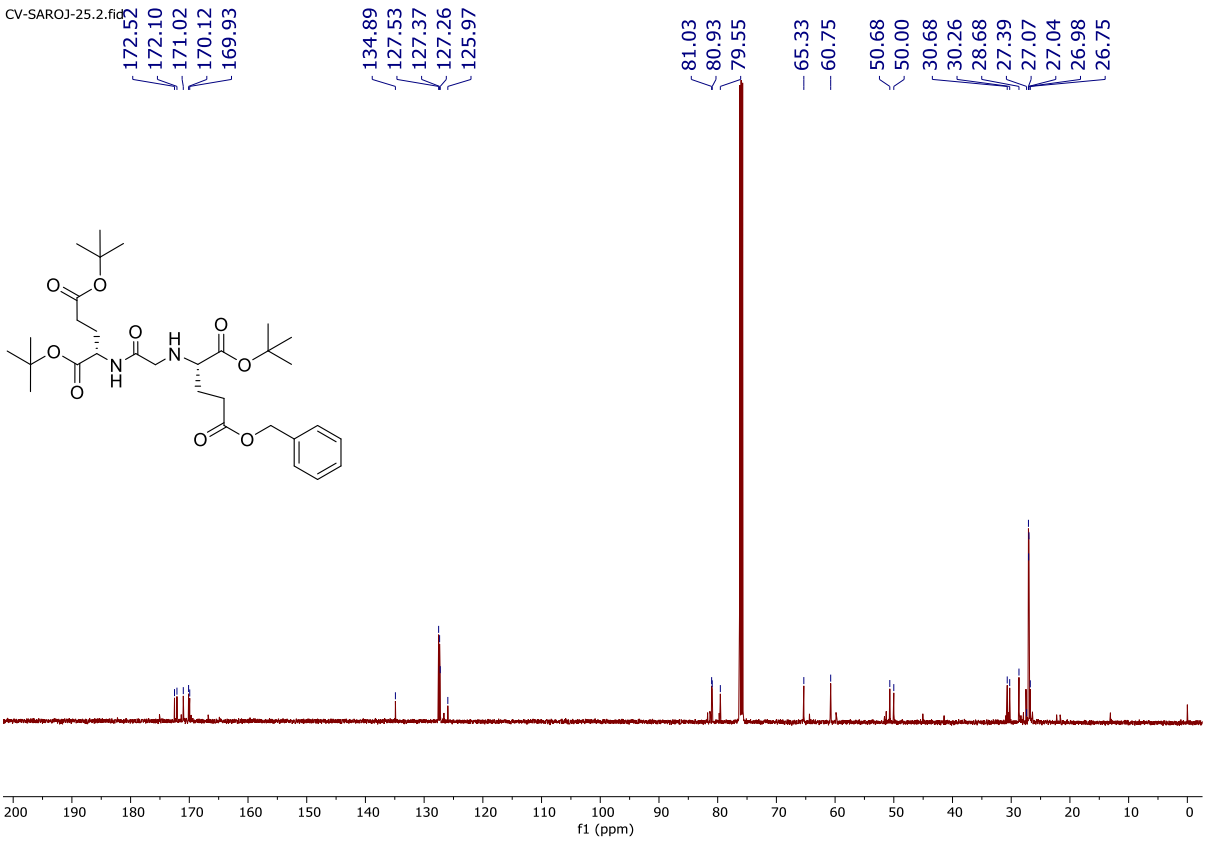

Figure 25. ^{13}C NMR spectrum (125 MHz) of **1a** in $CDCl_3$

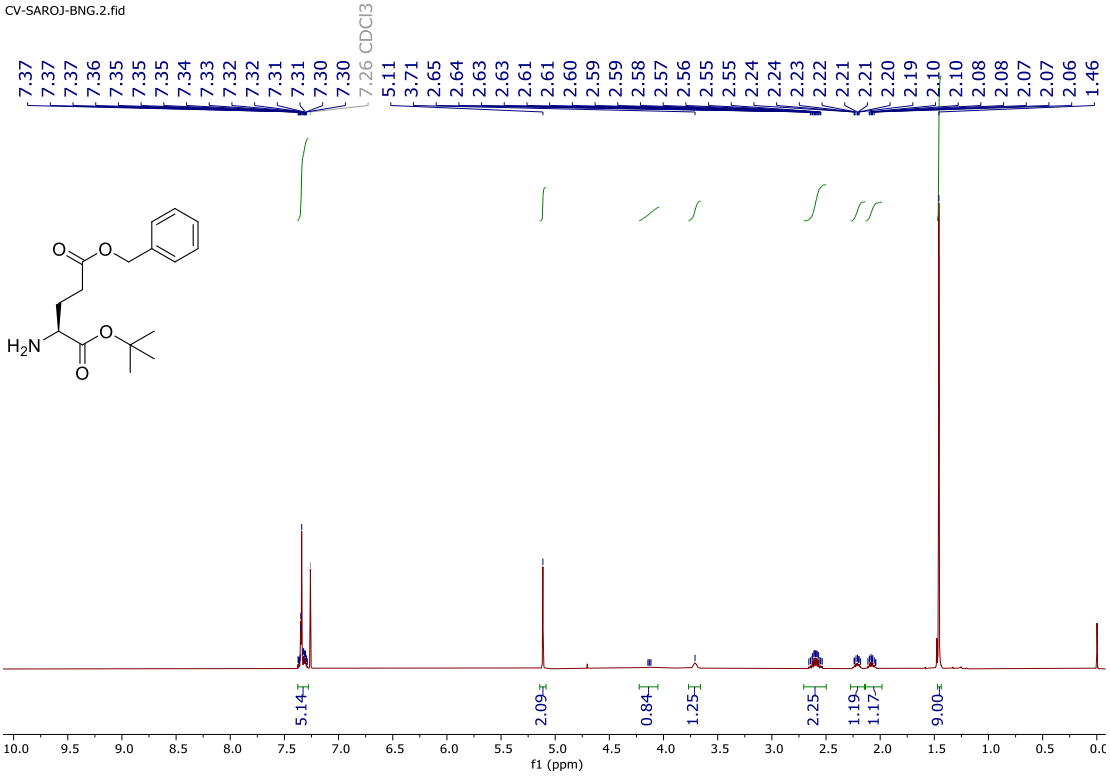

Figure 26. ^{1}H NMR spectrum (500 MHz) of **5** in $CDCl_3$

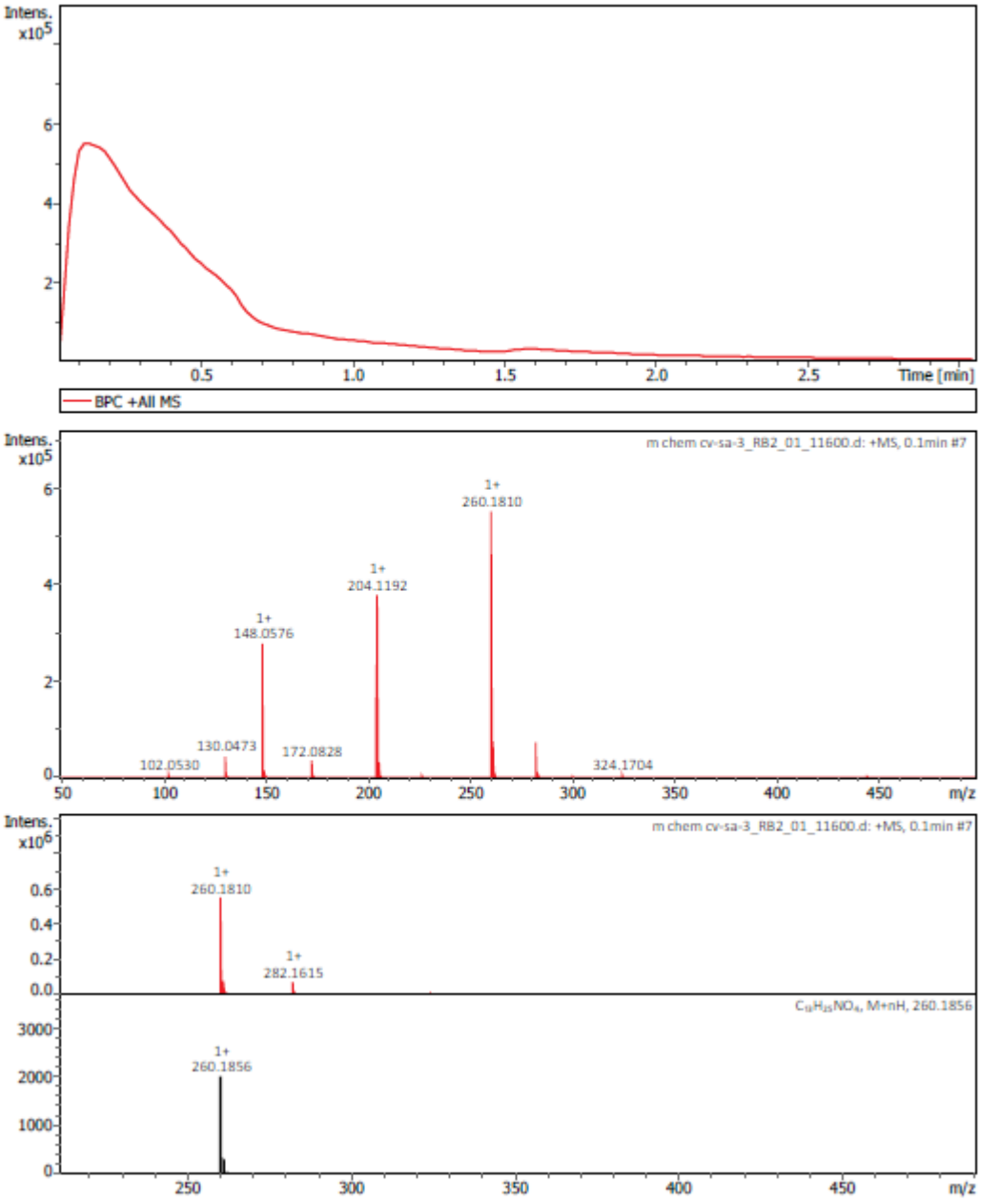

Figure 27. Mass spectrum of **4a** in MeOH

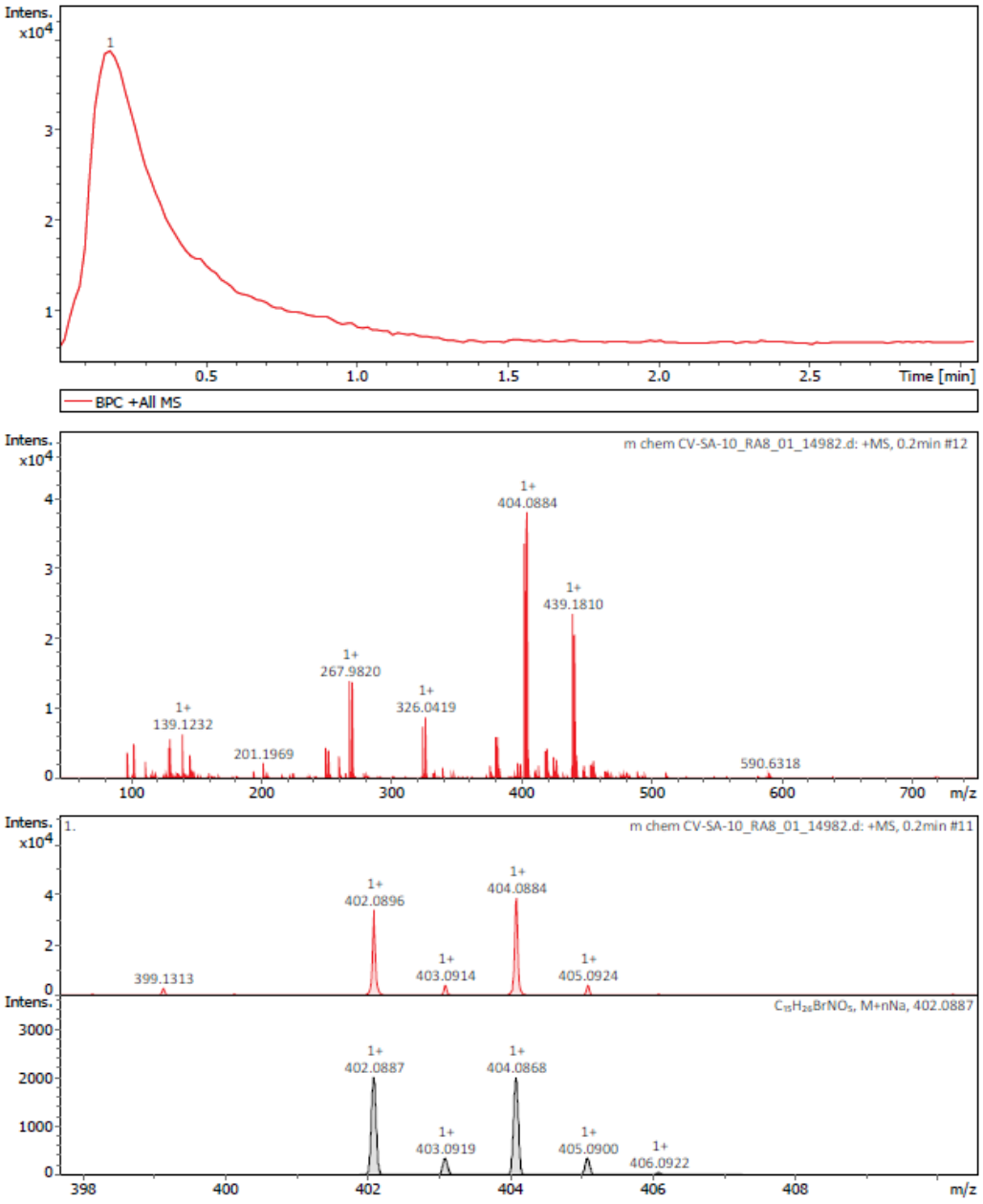

Figure 28. Mass spectrum of **3a** in MeOH

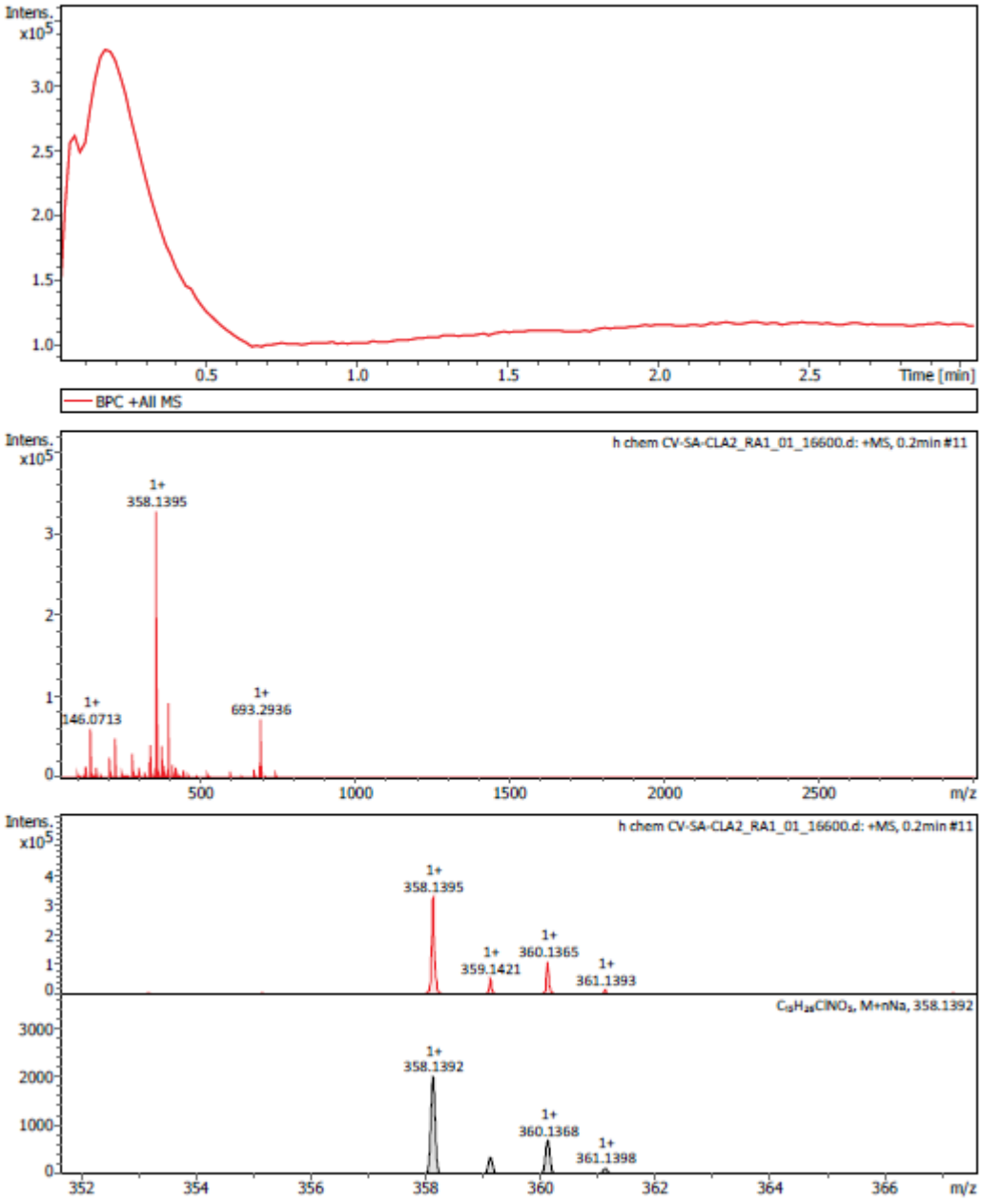

Figure 29. HRMS of **3a'** in MeOH

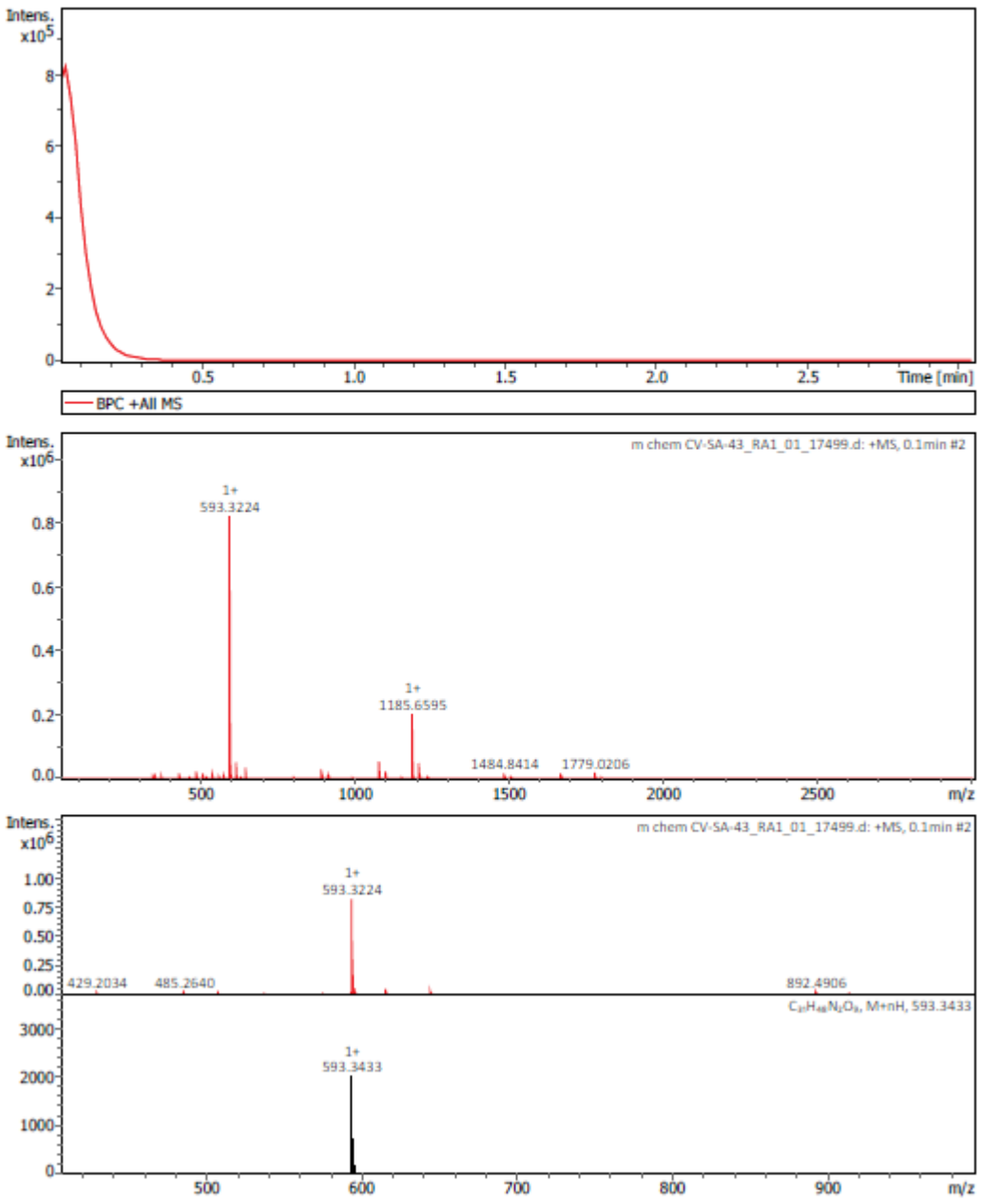

Figure 30. Mass spectrum of **1a** in MeOH

REFERENCES

1. Sung H., Ferlay J., Siegel R. L., Laversanne M., Soerjomataram I., Jemal A., Bray F. (2021), Global cancer statistics 2020: GLOBOCAN estimates of incidence and mortality worldwide for 36 cancers in 185 countries, CA Cancer J. Clin., 71, 209–249 (DOI: 10.3322/caac.21660).
2. Baskar R., Lee K. A., Yeo R., Yeoh, K. (2012), Cancer and radiation therapy: Current advances and future directions, Int. J. Med. Sci., 9, 193–199 (DOI: 10.7150/ijms.3635).
3. Kularatne S. A., Chelvam V., Santhapuram H. K. R., Wang K., Vaitilingam B., Henne W. A., Low P. S. (2010), Synthesis and biological analysis of prostate-specific membrane antigen-targeted anticancer prodrugs. J. Med. Chem., 53, 7767–7777 (DOI: 10.1021/jm100729b).
4. Chen K., Chen X. (2010), Design and development of molecular imaging probes, Curr. Top. Med. Chem., 10, 1227−1236 (DOI: 10.2174/156802610791384225).
5. Siegel R. L., Miller K. D., Fuchs H. E., Jemal A. (2021), Cancer Statistics, 2021, CA Cancer J. Clin., 71, 7–33 (DOI: 10.3322/caac.21654).
6. Mathur P., Sathishkumar K., Chaturvedi M., Das P., Sudarshan K. L., Santhappan S., Nallasamy V., John A., Narasimhan S., Roselind F. S. (2020), Cancer statistics, 2020: report from national cancer registry programme, India, JCO Global Oncology, 6, 1063–1075 (DOI: 10.1200/GO.20.00122).
7. Penson D. F., Litwin M. S. (2003), The physical burden of prostate cancer, Urol. Clin. N. Am., 30, 305–313 (DOI: 10.1016/S0094-0143(02)00187-8).
8. Katz A. (2007), Quality of life for men with prostate cancer, Cancer Nurs., 30, 302–308 (DOI: 10.1097/01.NCC.0000281726.87490.f2).
9. Zeller J. L. (2007), Grading of prostate cancer, JAMA, 298, 1596 (DOI: 10.1001/jama.298.13.1596).
10. Ghosh A., Heston W. D. (2004), Tumor target prostate specific membrane antigen (PSMA) and its regulation in prostate cancer, J. Cell Biochem., 91, 528–539 (DOI: 10.1002/jcb.10661).
11. Davis M. I., Bennett M. J., Thomas L. M., Bjorkman P. J. (2005), Crystal structure of prostate-specific membrane antigen, a tumor marker and peptidase, Proc. Natl. Acad. Sci. U S A., 102, 5981–5986 (DOI: 10.1073/pnas.0502101102).
12. Mesters J. R., Barinka C., Li W., Tsukamoto T., Majer P., Slusher B. S., Konvalinka J., Hilgenfeld R. (2006), Structure of glutamate carboxypeptidase II, a drug target

in neuronal damage and prostate cancer, EMBO J., 25, 1375–1384 (DOI: 10.1038/sj.emboj.7600969).

13. Rajasekaran A. K., Anilkumar G., Christiansen J. J. (2005), Is prostate-specific membrane antigen a multifunctional protein?, Am. J. Physiol. Cell. Physiol., 288, C975–C981 (DOI: 10.1152/ajpcell.00506.2004).
14. Liu H., Rajasekaran A. K., Moy P. (1998), Constitutive and antibody induced internalization of prostate-specific membrane antigen, Cancer Res., 58, 4055–4060.
15. Barinka C., Rojas C., Slusher B., Pomper M. (2012), Glutamate carboxypeptidase II in diagnosis and treatment of neurologic disorders and prostate cancer, Curr. Med. Chem., 19, 856–870 (DOI: 10.2174/092986712799034888).
16. Byun Y., Mease R. C., Lupold S. E., Pomper M. G. (2009), Drug design of zinc-enzyme inhibitors. Supuran C. T., Winum J.Y. (Ed) Recent development of diagnostic and therapeutic agents targeting glutamate carboxypeptidase II (GCPII). John Wiley & Sons, Inc. New York, pp. 881–910 (ISBN 9780470275009) (DOI:10.1002/9780470508169.ch36).
17. Jackson P. F., Cole D. C., Slusher B. S., Stetz S. L., Ross L. E., Donzanti B. A., Trainor D. A. (1996), Design, synthesis, and biological activity of a potent inhibitor of the neuropeptidase N-acetylated α-linked acidic dipeptidase, J. Med. Chem., 39, 619–622 (DOI: 10.1021/jm950801q).
18. Mease R. C., Dusich C. L., Foss C. A., Ravert H. T., Dannals R. F., Seidel J., Prideaux A., Fox J. J., Sgouros G., Kozikowski A. P., Pomper M. G. (2008), N-[N-[(S)-1,3-Dicarboxypropyl]carbamoyl]- 4-[^{18}F]-fluorobenzyl-L-cysteine, [^{18}F]DCFBC: a new imaging probe for prostate cancer, Clin. Cancer Res., 14, 3036–3043 (DOI: 10.1158/1078-0432.CCR-07-1517).
19. Maresca K. P., Hillier S. M., Fernia F. J., Keith D., Barone C., Joyal J. L., Zimmerman C. N., Kozikowski A. P., Barrett J. A., Eckelman W. C., Babich J. W. (2009), A series of halogenated heterodimeric inhibitors of prostate specific membrane antigen (PSMA) as radiolabeled probes for targeting prostate cancer, J. Med. Chem., 52, 347–357 (DOI: 10.1021/jm800994j).
20. Graham K., Lesche R., Gromov A. V., Böhnke N., Schäfer M., Hassfeld J., Dinkelborg L., Kettschau G. (2012), Radiofluorinated derivatives of 2-(phosphonomethyl) pentanedioic acid as inhibitors of prostate specific membrane antigen (PSMA) for the imaging of prostate cancer, J. Med. Chem., 55, 9510−9520 (DOI: 10.1021/jm300710j).

21. Sengupta S., Krishnan M. A., Dudhe P., Reddy R. B., Giri B., Chattopadhyay S., Chelvam V. (2018), Novel solid-phase strategy for the synthesis of ligand-targeted fluorescent-labelled chelating peptide conjugates as a theranostic tool for cancer, Beilstein J. Org. Chem., 14, 2665–2679 (DOI: 10.3762/bjoc.14.244).
22. Krishnan M. A., Chelvam V. (2021), Developing μSpherePlatform Using a Commercial Hairbrush: An agarose 3D culture platform for deep-tissue imaging of prostate cancer, ACS Appl. Bio Mater., 4, 4254−4270 (DOI: 10.1021/acsabm.1c00086).
23. Chen Y., Dhara S., Banerjee S. R., Byun Y., Pullambhatla M., Mease R. C., Pomper M.G. (2009), A low molecular weight PSMA-based fluorescent imaging agent for cancer, Biochem. Biophys. Res. Commun., 390, 624–629 (DOI: 10.1016/j.bbrc.2009.10.017).
24. Krishnan M. A., Yadav K., Roach P., Chelvam V. (2021), A targeted near-infrared nanoprobe for deep-tissue penetration and imaging of prostate cancer, Biomater. Sci., 9, 2295–2312, (DOI: 10.1039/D0BM01970D).
25. Banerjee S. R., Foss C. A., Castanares M., Mease R. C., Byun Y., Fox J. J., Hilton J., Lupold S. E., Kozikowski A. P., Pomper M. G. (2008), Synthesis and evaluation of technetium-99m- and rhenium-labeled inhibitors of the prostate-specific membrane antigen (PSMA), J. Med. Chem., 51, 4504–4517 (DOI: 10.1021/jm800111u).
26. Banerjee S. R., Pullambhatla M., Byun Y., Nimmagadda S., Green G., Fox J. J., Horti A., Mease R. C., Pomper M. G. (2010), ^{68}Ga-Labeled inhibitors of prostate-specific membrane antigen (PSMA) for imaging prostate cancer, J. Med. Chem., 53, 5333−5341 (DOI: 10.1021/jm100623e).
27. Banerjee S. R., Pullambhatla M., Foss C. A., Nimmagadda S., Ferdani R., Anderson C. J., Mease R. C., Pomper M. G. (2014), ^{64}Cu-Labeled inhibitors of prostate-specific membrane antigen for PET imaging of prostate cancer, Bioconjugate Chem., 57, 2657–2669 (DOI: 10.1021/jm401921j).
28. Krishnan M. A., Pandit A., Sharma R., Chelvam V. (2021), Imaging of prostate cancer: Optimizing affinity to prostate specific membrane antigen by spacer modifications in a tumor spheroid model, J. Biomol. Struct. Dyn., 27, 1–22 (DOI: 10.1080/07391102.2021.1936642).